Wake flow lab measurements of multi-rotor wind turbines

Andreas Grodås Jørs

Torbjørn Løvik Mjåtveit

Bachelor's thesis in Energy technology

Bergen, Norway 2021

Høgskulen på Vestlandet

Western Norway University of Applied Sciences

Wake flow lab measurements of multi-rotor wind turbines

Andreas Grodås Jørs

Torbjørn Løvik Mjåtveit

Department of Mechanical- and Marine Engineering

Western Norway University of Applied Sciences

NO-5063 Bergen, Norway

IMM 2021 M69

Høgskulen på Vestlandet

Fakultet for Ingeniør- og Naturvitskap

Institutt for maskin- og marinfag

Inndalsveien 28

NO-5063 Bergen, Norge

Cover and backside images © Norbert Lümmen

Norsk tittel:	Lab målinger av kjølvannstrømninger til multirotor vindturbiner
Author(s), student number:	Andreas Grodås Jørs, 580839 Torbjørn Løvik Mjåtveit, 580835
Study program:	Energy technology
Date:	05.2021
Report number:	IMM 2021-M69
Supervisor at HVL:	Jan Michael Simon Bartl
Assigned by:	HVL
Contact person:	Jan Michael Simon Bartl
Number of files delivered:	1/2

Preface

This bachelor thesis is written at the Department of Mechanical and Marine Engineering for the Western University of Applied Sciences (WNUAS), as part of the Bachelor program in Energy Technology. Our internal supervisor was Jan Michael Simon Bartl.

We would like to express our gratitude to Jan Michael Simon Bartl for his advising and guidance, both in the writing process and for the experiment in Marine lab. We would also like to thank Chief Engineer Harald Moen and his staff for help with the experimental setup.

Abstract

There is an increasing need for renewable energy in the world, and wind energy is one of the main sources to satisfy this demand. Multi-rotor wind turbines are in this bachelor thesis analysed to see if they can be a viable replacement for massive single-rotor turbines. This is done by conducting wake measurements at different downstream distances in the Marine lab at HVL. Rotors were arranged in a four- and seven-disc setup using simplified actuator discs, to generate good and comparable baseline data. In our results, the wakes of multi-rotors were found to recover faster and have lower velocity deficits in the near wake compared to the single-rotor. However, further downstream the wake of multi-rotors recover slower due to lower turbulence, resulting in rather similar velocity deficits in the far wake region for all turbine types. The seven-disc turbine was in addition tested with different inter-rotor spacing to see how upstream blockage, inter-rotor jet streams, and turbulent mixing influence the wake. From experimental results, a significantly lower velocity deficit is measured in the near wake region when increasing the spacing between the discs. Similarly, the turbulence was also reduced, which could lead to lower fatigue loads on potential downstream turbines. It was also found that with no spacing a multi-rotor wake almost looks identical to that of a single-rotor. Therefore, spacing between the discs proves to be one of the most important features of a multi-rotor turbine, which ensures a fast wake recovery.

Sammendrag

Behovet for fornybar energi øker globalt, og vindkraft er en av hovedkildene til å oppnå dette. Multirotor vindturbiner blir i denne bachelor oppgaven analysert for å se de kan være en levedyktig erstatning til enorme enkeltrotor vindturbiner. Dette er gjennomført ved å undersøke kjølvann målinger ved forskjellige nedstrøms avstander i Marinlabben på HVL. Rotorene var arrangert i oppsett på fire og syv disker gjennom bruk av forenklede aktuator disker, for å frembringe god og sammenlignbar data. Våre målinger viser at kjølvannet til multirotorer regenererer raskere og har lavere hastighetstap enn singlerotorer i fremre del av kjølvannstrømningen. Lengre nedstrøms regenerer hastigheten til multirotorer saktere grunnet lavere turbulens enn singlerotoren. Dette resulterer i at alle turbintypene har noenlunde samme hastighetstap langt bak i kjølvannet. For turbinen med syv disker var det i tillegg testet med forskjellig mellomrom for å finne ut hvordan blokkasje, jetstrømmer, og miksing påvirker kjølvannet. Med økt avstand mellom diskene, er det målt et betydelig lavere hastighetstap rett bak rotoren. På samme måte er turbulensen redusert, noe som kan resultere i lavere utmattelsesbelastninger for turbiner nedstrøms. Det er også funnet ut at uten avstand mellom diskene er kjølvannet nesten identisk som en singlerotor. Mellomrom mellom diskene har derfor vist seg å være en av de viktigste faktorene til en multirotor turbin.

Table of contents

1 Introduction

In recent years, a high focus on climate has contributed to several domestic and international treaties aiming to reduce our carbon footprint. Forcing both countries and companies into action. Among many, the Paris agreement is seen upon as the most important treaty, in which The European Commission has its own response. To limit the world's temperature increase, their aim is to be climate-neutral by 2050. Renewable energy resources will play a pivotal role in reaching that goal, where one of the most prominent options is wind energy and in particular offshore wind. Their proposed strategy is therefore to "increase Europe's offshore wind capacity from its current level of 12 GW to at least 60 GW by 2030 and to 300 GW by 2050." [1]

> *The European Commission estimates between 240 and 450 GW of offshore wind power is needed by 2050 to keep temperature rises below 1.5°C. Electricity will represent at least 50% of the total energy mix in 2050 and 30% of the future electricity demand will be supplied by offshore wind.* [2]

Within the wind power industry, there is a shifting focus towards offshore wind turbines as opposed to onshore. This is mainly due to better wind conditions, but also due to the NIMBY (Not In My Back Yard) principle. In the last decades, there has also been a major increase in the size of wind turbines. Introducing us to multimegawatt structures. This leads to distinct issues concerning the economic and practical feasibility. With turbine blades reaching more than 100 meters in length, the size and weight become hard to handle. New factories and equipment are needed to produce components of such scale. Being able to mount the finished structures is not an easy task either. At one point this expansion is bound to stagnate.

This raises the question of whether not multiple smaller rotors installed on only one floating offshore structure could significantly reduce the levelized cost of energy (LCOE) for an offshore wind power plant. By making several smaller components, the manufacturing becomes more comprehensible, transport is easier, and assembly can be done with smaller machinery. Another well-known problem in offshore wind farms is the single turbine's wake flow interaction. For an economically optimized farm, it is desirable to install the turbines as tight as possible, but the impact on wake flows causes lower power extraction and increased fatigue loads for downstream turbines. Multi-rotor systems (MRS) can therefore potentially provide several benefits over single-rotors, by increasing mixing processes in the wake flow which allow for a faster wake recovery.

Jamieson and Branney [3] brought up the topic of multi-rotors in recent years. They investigated the interplay of weight and energy capture in multi-rotors and identified potential benefits for multi-rotor concepts, in terms of costs. While later investigating structural considerations of the same system [4]. Wider research of structural benefits for different types of concepts was just recently published by Störtenbecker et al. [5]. Strengthening the claim that an increasing number of rotors decreases the LCOE. At the Technical University of Denmark (DTU), a 4-rotor concept turbine from Vestas delivering 900 kW was in operation from 2016-2018 [6]. vdLaan et al. [7] ran numerical simulations of the Vestas multi-rotor demonstrator (4R-V29)

and compared the results against field measurements with regards to power performance and wake deficit. Showing a calculated 0-2% and a measured 1.8% power increase at below rated wind speed. The study also found that the wake recovery distance is 1.03– 1.44 D_{eq} shorter than an equivalent single-rotor and has a lower added turbulence in the far wake. This is an important feature which potentially can lead to closer wind turbine spacing. Furthermore, vdLaan et al. [8] conducted research to calculate the effects of multi-rotor turbines within a wind farm. This was done by performing a reynolds averaged navier stokes (RANS) simulation of a rectangular 4x4 wind farm layout, for both multi-rotor and single-rotor. Ranging from 0.3%-1.7% increase in annual energy production, the multi-rotor yields more energy than the equivalent single-rotor. Ghaisas et al. [9] carried out a similar study by using large-eddy simulations (LES) and actuator drag-disc model. A baseline 1-rotor and 4-rotor simulation was performed but had an additional five-row setup in the streamwise direction with a 4D spacing between. They reached a matching conclusion, where the multi-rotor turbine wakes are found to recover faster. In a wind farm arrangement, the wake losses are also found to be significantly smaller.

This leads us to our thesis question: **Can a multi-rotor system reduce the wake flow deficit compared to a single-rotor and prove beneficial in a wind farm arrangement, and how will the multi-rotor number and spacing affect the results?**

The proposed project is aiming to investigate how different design parameters such as number, size, and formation in a multi-rotor setup are influencing the mean and turbulent wake flow. After a theoretical rotor and wake design approach is used, different multi-rotor concepts are to be tested in a lab-scale experiment with porous rotor discs in the towing tank of Marin Lab at HVL. The experimental data will be compared against Bastankhah et al. [10] to give a better validation of the result, as it shows the correlation between advanced simulation data and practical experiment implementation.

2 Theory

To get a better understanding of the contents in this bachelor thesis, a thorough theory is explained for the interaction of wind turbine wakes. Essential knowledge on the one-dimensional momentum theory, and how fundamental flow phenomena differs between single-rotors and multi-rotors are needed to understand the development of the wake.

2.1 Actuator disc

To simplify experiments and make results more comparable, a standardised actuator disc can be used as an idealized tool to simulate a turbine. An issue within experimental research is the possibility to compare results across different test facilities and objects. Every lab will have its own setup and configuration, meaning the same test done at different locations might have different results. By also using various object geometries, accurate comparisons are difficult. A solution to the problem is the implementation of standardised actuator disc shown in Figure 2-1. The simple design makes it easy to produce, meaning it does not need transporting for testing at other facilities.

The structural design of the porous disc imitates a real turbine by being denser closer to the centre. Just like a turbine has a thicker blade at the hub, than at the tip. There are pros and cons to the disc approach. While contributing to generate good baseline results, it cannot produce tip- and root vortices which affect the wake. The aforementioned disc has a solidity of around 60% [11] and the thrust coefficient is in experiments measured to stabilise at roughly 0.87 [12].

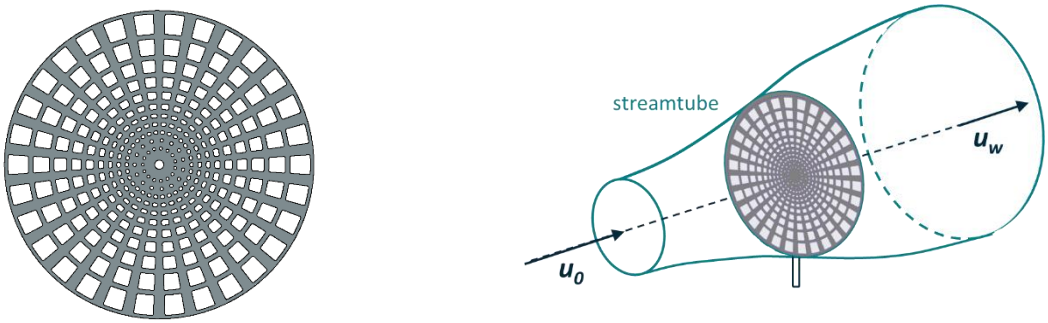

Figure 2-1: Actuator disc.

The one-dimensional momentum theory, also known as the actuator disc theory, is a fundamental way to understand how a wind turbine extracts kinetic energy from the wind. In this theory, the rotor is assumed to be an ideal disc, and the flow is inviscid. This means that there is no skin friction, and the maximum amount of power is extracted from the wind. At a short upstream distance from the disc, the velocity starts to decrease and continues to decrease until the pressure stabilizes. From the Bernoulli principle, a decrease in velocity leads to an increase in pressure. At the disc, the pressure has a drop as shown in Figure 2-2. Far downstream the pressure returns to atmospheric pressure, and the wind speed stops decreasing. At a short upstream distance from the disc, the velocity starts to decrease and continues to decrease until the pressure stabilises. [13]

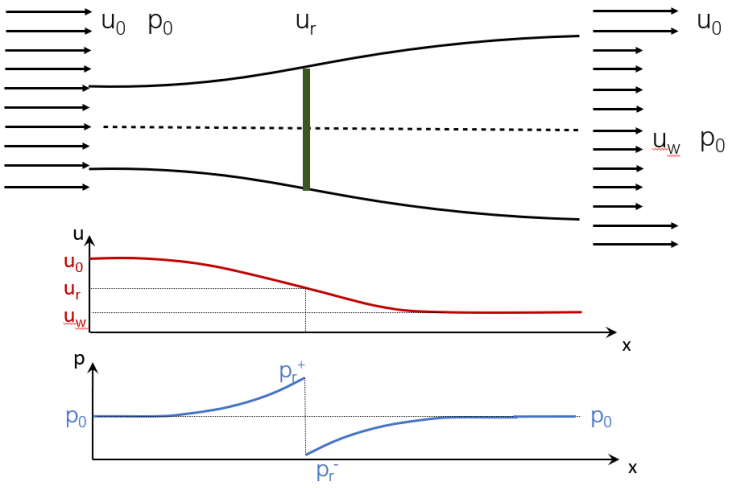

Figure 2-2: One-D momentum theory. Velocity and pressure development at the rotor.

How the pressure and velocity changes from far upstream to far downstream can be analysed by the Bernoulli equation. If a streamline is followed from upstream to the rotor, and from the rotor to far downstream, equation (1) and (2) is made.

$$P_0 + \frac{1}{2}\rho u_0^2 = P_r^+ + \frac{1}{2}\rho u_r^2 \qquad (1) \qquad P_r^- + \frac{1}{2}\rho u_r^2 = P_0 + \frac{1}{2}\rho u_w^2 \qquad (2)$$

With these two expressions the total pressure difference is derived in formula (3).

$$\Delta P = \frac{1}{2}\rho(u_0^2 - u_w^2) \qquad (3)$$

The pressure difference from far upstream to far downstream of the rotor, combined with mass and momentum conservation gives the velocity in the rotor plane. The axial induction factor a can be described as the ratio of the velocity reduction far upstream to the velocity at the rotor plane. This results in formula (4).

$$u_r = \frac{1}{2}(u_0 + u_w) = (1-a)u_0 \qquad (4)$$

The incoming wind speed meets the rotor with a force. According to Newton's third law, the rotor must meet this force with equal magnitude and opposite direction. This is called the thrust force and can be noted as pressure difference times the area of the rotor. The thrust force and the thrust coefficient are expressed in formula (5) and (6).

$$F_T = \Delta P A_r = \frac{1}{2}\rho A_r u_0^2 C_T \qquad (5) \qquad C_T = 4a(1-a) \qquad (6)$$

The power equation for a wind turbine is how much energy that is extracted from the wind presented in formula (7), and the power coefficient expressed in formula (8).

$$P = \frac{1}{2}\rho A u_0^3 C_P \qquad (7) \qquad C_P = 4a(1-a)^2 \qquad (8)$$

2.2 Blockage and Betz limit

When a body is placed in a channel or a wind tunnel it causes an acceleration of the velocity. This happens because of blockage, which is defined by how much area is blocked compared to the freestream area. For a wind turbine, the cross-sectional area is small compared to the area of the incoming wind speed. Whereas in a tidal channel the area is limited by the seabed and the water surface, making the blockage ratio more sensitive for increase. Figure 2-3 illustrates the flow around two neighbouring actuator discs, where a jet stream occurs in the centre. With an increasing blockage ratio due to the presence of rotors, the bypass flow accelerates. This leads to an increase in pressure difference at the rotor plane, which makes the power output of the turbine reach a higher level. On the other hand, if the blockage ratio is too high the flow will slow down and reduce the power output. Therefore, the number of turbines in a channel is limited. [14]

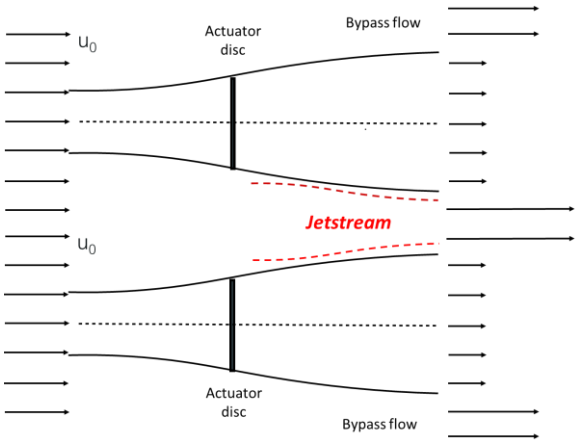

Figure 2-3: Jet stream and bypass flow on closely spaced actuator discs.

The upper limit for power extraction by a wind turbine is known as the Betz limit. If formula (8) is differentiated the highest value of a is found to be 1/3.

$$\frac{dC_P}{da} = 4(1-a)(1-3a) = 0$$

If the value of 1/3 is put into formula (8) it gives a value of 2/3 for C_P. This is the maximum kinetic energy that can be captured from the wind. A fence of turbines in a tidal channel can get increased power output because of blockage. The increase in power leads to an exceedance of the Betz limit, and a new upper limit of power extraction is found. This is called the Lanchester-Betz limit which has a value of 79.8%. To reach this power limit, 40% of the tidal channel must be blocked.[15]

Increased power output due to blockage is not only related to turbines in a tidal channel. Recent wind tunnel experiments have shown that by placing three turbines with a lateral distance of 0.25D or 0.5D the total power output can be increased, compared to when the three turbines are standing alone. [16] Another experiment has been performed with a lateral distance of 3D. This experiment was done with CFD simulation. By varying the inflow angle of the incoming wind speed, the maximum power production compared to a standalone wind turbine was a 2% increase.[17] These results show that the blockage effect has an influence on power production for lateral closely spaced wind turbines.

2.3 Multi-rotor

There are only a few multi-rotor concepts currently tested. An example is the Vestas four-rotor turbine [7]. One of the challenges is that with the increased number of parts in the system, there is a higher chance of failure for one rotor. On the other hand, when one turbine is down the others is still producing power and thereby the chance of downtime is lower. This is not a possibility for single-rotors. The fact that a multi-rotor consist of more parts give the opportunity to mass-produce, which results in lower unit cost. [18] Another advantage is that the total aerodynamic load is less when the load is better distributed among each of the single-rotors. Since each rotor is smaller it is possible to individually control it to spatial variations in incoming wind speed [3].

If a single-rotor and a multi-rotor with equivalent power are compared, the mass and cost of rotor and drivetrain can be calculated by $1/\sqrt{n}$, where n is the number of rotors in the system. Thus, a nine-rotor turbine would cost 1/3 of the single-rotor. This shows that with increasing rotor number, mass and weight reduction have a huge potential. Jamieson et al. [3] did a lifetime cost comparison of a 20 MW single-rotor turbine with a MR45 turbine which consisted of 45x444kW turbines, delivering a total of 20 MW. The largest cost category in this lifetime analysis is installation costs, which counted for 42% of the overall turbine cost. The MR45 and the single-rotor had a 5.6% difference in installation cost in favour of MR45. A multi-rotor consists of more parts and a more complex structure, but the mass is significantly reduced. Although the multi-rotor consists of more parts, operation and maintenance cost was 28,6% lower than the single-rotor. In total the multi-rotor had a 30% cost reduction compared to the single-rotor. A multi-rotor with fewer rotors in the system will have a smaller cost reduction since it increases with number, but the cost reduction is still significant. An example of this is the total lifetime cost for a MR4, which is 80% of a single-rotor. These cost analyses are sensitive to many suppositions, therefore the need for more research on the subject is present. [3]

Petros Chasapogiannis et al. [19] have done CFD simulations on the performance of a MR7 actuator disc turbine, with a rotor spacing of 0.05D. They found a 1.17% increase in thrust and a 3.15% increase in power compared to a single-rotor. The increase is arguably due to blockage, and it shows that a multi-rotor system will not have lower power production compared to a single-rotor system. They also did a vortex model simulation which took the blade geometry and rotation of the blades into account. These results gave only a small increase in thrust and a slight decrease in power. The actuator disc simplification therefore gave realistic results. [19]

2.4 Turbulence

Flow can be divided into laminar- and turbulent flow. When fluid flows in parallel layers with no disruption, there is laminar flow. Whereas turbulent flow has a chaotic change in pressure and velocity. Turbulence can be defined as a velocity gradient in time, as opposed to wind shear which is a velocity gradient for a given direction.

$$Shear = \frac{\partial u}{\partial z} \tag{9}$$

$$Turbulence = \frac{du}{dt} \tag{10}$$

Turbulence and wind shear are important for wind turbines due to their impact on the turbine- and wind farm performance. The flow phenomena occur naturally in the atmospheric boundary layer, which can be divided into three categories depending on flow characteristics.

Stable atmospheric boundary layer has high wind shear but low turbulence intensity (low mixing).

Neutral atmospheric boundary layer has medium wind shear and medium turbulence intensity (medium mixing).

Unstable boundary layer has low wind shear, but high turbulence intensity (high mixing).

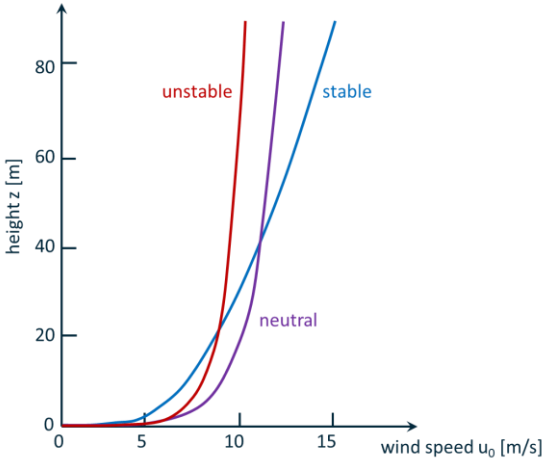

Figure 2-4: Atmospheric boundary layers.

The different boundary layers have both pros and cons. Turbulence gives higher mixing which again provides faster wake recovery. Wind shear is on the other hand a contributor to turbulence and might be positive for the wake as well. Another aspect to consider is the impact on the structure's lifetime. Higher turbulence and shear forces have more wear and tear, which consequently can lead to reduced lifetime and performance. This especially counts for large wind turbines, where the upper and lower part can experience substantially different flow velocities due to vertical wind shear. [20]

Turbulence can be differentiated between inflow conditions and rotor added turbulence. While inflow conditions are the incoming flow, rotor added is turbulence produced by the rotor. It can be presented in several ways. Turbulence intensity (TI) is velocity standard deviation divided by average velocity. Results can be given in decimals or as a per cent if multiplied by a hundred in formula (11). TI can generally be divided into low (<1%), medium (1%-5%), and high (>5%) intensity, but a TI of less than one present is normally only achieved in laboratories like wind tunnels. [21]

$$TI = \frac{\sigma_u}{\bar{u}} \ ([-] \ or \ [\%]) \tag{11}$$

Turbulent kinetic energy (tke) is half the sum of variances. In other words, the standard deviation squared in x, y and z direction divided by two. This is shown in formula (12). The source of the formula stems from specific kinetic energy given in formula (13), where velocity is replaced by variance.

$$tke = \frac{1}{2}\left(\overline{(u')^2} + \overline{(v')^2} + \overline{(w')^2}\right) \tag{12}$$

$$e = \frac{1}{2}u^2 \tag{13}$$

In cases where the turbulence is isotropic, a simplification of the formula can be used. This assumes the variance is equal in all direction, and only one direction is therefore needed to calculate the turbulent kinetic energy. This can for example be used in the far wake, where the flow is fully mixed. The abbreviated formula is given in (14) using x-direction.

$$tke = \frac{3}{2}\overline{(u')^2} \tag{14}$$

2.5 Wake

As long as there is flow, there will always be a wake behind a wind turbine. It is a complex phenomenon dependent on several factors. Including blade design, blade number, wind speed, topography, atmosphere, and height. The main concern with wake flows is the major turbulence increase and velocity deficit behind the turbine. For a single structure, the effect is of no importance but in a wind farm arrangement, an upstream turbine's wake results in lower windspeed for downstream turbines.

2.5.1 Single-rotor wakes

Depicted in Figure 2-5 (a) is a figure showing two essential vortical formations, tip- and root vortices, which form into helixes. They arise by virtue of rotation. The disturbance in streamwise direction is amplified as the vortices decay into turbulence.

Wakes are often divided into three sections. Near-, transition-, and far wake. The distinct differences are the velocity deficit and turbulence intensity. Near wake is also called the turbulence production region and can be described with high turbulence intensity and low flow velocity. At some point, the wake will start to recover and stabilize itself. This can be identified as the transition area. In this section, the turbulence is more scattered which causes higher mixing in the wake. As a result, the flow velocity is still low but more uniform. Within the far wake, velocities regain towards inflow conditions and turbulence is reduced. A second turbine is commonly placed in this area due to lower exerted forces and higher velocities, leading to increased lifetime and extracted energy.

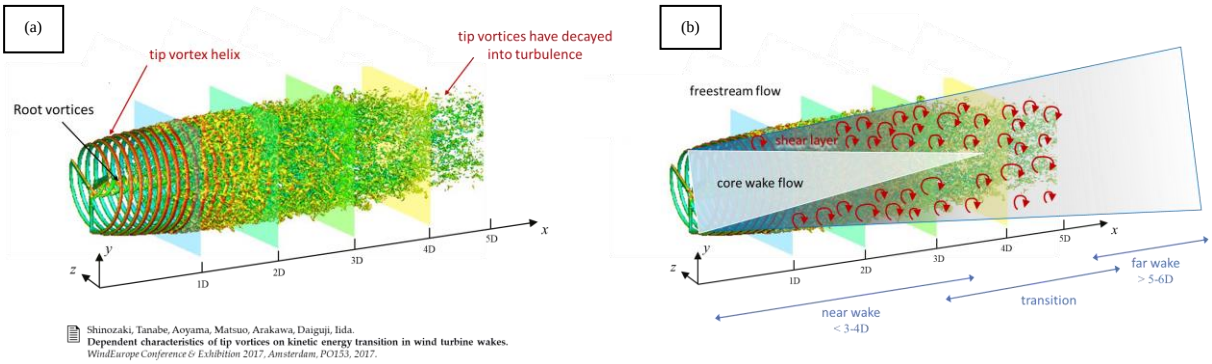

Figure 2-5: (a) Wake flow phenomena. (b) Sectioning and turbulence.

By replacing a wind turbine with a non-rotating actuator disc, tip and root vortices are no longer present. This causes some differences in the flow, but it will still behave similarly. [11] At the edge of the wake, a shear layer is formed, separating it from the free stream flow. With high velocity differences, the shear gradient produces eddies to equalize the dissimilarity. This is the main contributor to turbulence in the wake for both wind turbine and actuator disc. Figure 2-5 (b) and Figure 2-6 (a) illustrates this effect.

2.5.2 Dual and multi-rotor wake

The wakes behind dual and multi-rotor setups differ from single-rotors. Their main contributor to turbulence is still shear gradients, but several other flow phenomena affect the wake. As mentioned in section 2.2, jet streams and blockage effects have a significant impact. Just how large, will be investigated in this study. In Figure 2-6 a theoretical illustration comparing a single-rotor against a four-rotor setup is shown. The single-rotor has turbulence production on both sides of the disc, which eventually culminate into uniform turbulence along the cross-section. Meanwhile, the multi-rotor sees turbulence on either side but also and in the centre of the cross-section. This contributes to higher mixing in the near wake of the turbine, with higher turbulence intensity. Although this might seem bad, it allows for a faster regain of the wake. In a wind farm arrangement, this could mean more closely spaced turbines. The illustration and theory are also valid for a dual rotor. In a LES study performed by Bastankhah et al. [10], a MR4 turbine proved to yield far higher turbulence intensity in the wake 2D downstream compared to a single-rotor. Furthermore, it also experienced a lower velocity deficit. On the other hand, at 4D downstream the turbulence intensity had already reduced below single-rotor levels. Meanwhile, the single-rotor showed increasing values. This contributed to faster recovery for the MR4 wake.

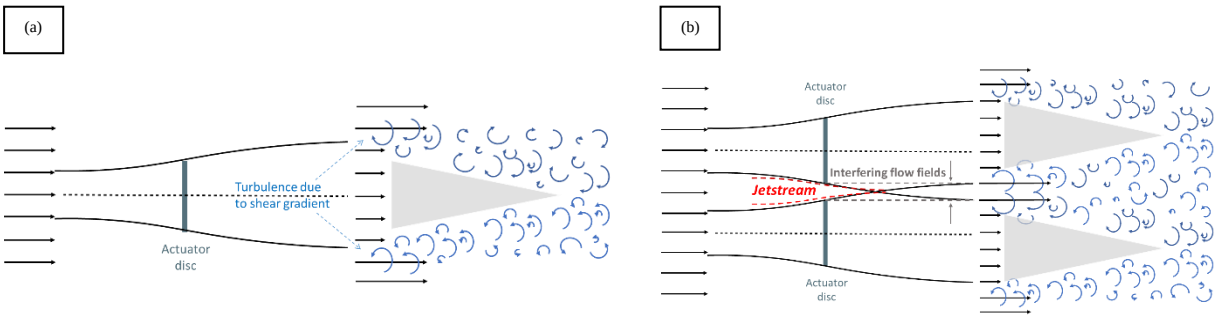

Figure 2-6: Turbulence production due to shear gradient behind: (a) A single-rotor setup. (b) A dual or MR4 setup. Notice that figure b has turbulence production in the centre of the structure, which gives higher mixing.

2.5.3 Wake flow in water

While wind turbines have existed for decades and continuously increases their market share, tidal stream turbines have not yet been fully implemented. Geometry-wise they are very much alike but utilizes two vastly different mediums for power extraction. While water has a density of approximately 1000kg/m^3, air is over 800 times lighter with a density of around 1.225kg/m^3. Tidal stream turbines also operate under lower flow velocities than wind turbines and have a smaller size. This begs the question of whether a small-scale towing tank experiment with an actuator disc really is representative for a full-scale wind turbine.

2.5.3.1 Scaling

Small scale testing with actuator discs is a good and economic approximation to full-scale turbine models, but its uses are limited. For measuring flow phenomena, comparing setups, effects of yaw angle, multi-rotor systems etc, it can be a great tool, but only as a baseline pinpointer for further testing. It can never replace the value of actual wind turbine data.

Several elements need to be considered when pursuing a disc scaling approach. Firstly, the Reynolds number given in equation (15).

$$Re = \frac{\rho v d}{\mu} \tag{15}$$

It is a dimensionless value where ρ stands for fluid density, v is velocity, d is diameter, and μ is fluid viscosity. Modern day wind turbines rise above a staggering 200 meters in diameter, with Haliade-X holding the current record of 220 meters. The model scale disc is on the contrary only 0.2 meter. This gives a scaling factor of 1100. Increasing the size of a wind turbine also increases the corresponding Reynolds number. An article from Ge et al. [22] found that airfoils with higher Reynolds number exhibited better performance at a given angle of attack, such as a higher lift-to-drag ratio. The optimal blade design would therefore change with size and Reynolds number. A small-scale model would accordingly so behave differently. Since this experiment is done in a water tank, the diameter is not changeable. Although the tank itself could withhold a larger disc, interference from the walls could become an issue. Viscosity and density are also different when performing the experiment in water. With equal diameter and velocity, the Reynolds number would be higher in water than air. This counteracts some of the difference in size but to prevent stern wave production and bending, the velocity used needs to be much lower. In the work by Hansen et al. with the same setup, a velocity of only 0.4 m/s was found to be ideal. [12] In Equation 1, two calculations are executed to show the differences between air and water with regards to Reynolds number and a third for scaled model comparison. The calculations prove that there are insignificant differences by changing the medium if the velocity is changed accordingly. Hence experimenting in water is a valid comparison to air. The only concern is the reduced size of the scale model which corresponds to a lower Reynolds number. This will always be an issue with small-scale testing, but it is reasonable to believe that the results are similar, although not fully optimal.

(a)

$$Re_D, fs_A = \frac{1.225\frac{kg}{m^3} * 10\frac{m}{s} * 220m}{1.825 * 10^{-5}\, Pa \cdot s} = 14.8 * 10^7$$

(b)

$$Re_D, fs_W = \frac{1000\frac{kg}{m^3} * 0.5\frac{m}{s} * 220m}{1 * 10^{-3} Pa \cdot s} = 11 * 10^7$$

(c)

$$Re_D, ms_W = \frac{1000\frac{kg}{m^3} * 0.5\frac{m}{s} * 0.2m}{1 * 10^{-3} Pa \cdot s} = 10 * 10^4$$

Equation 1: Reynolds number calculation for (a) reference turbine in air. (b) Reference turbine in water with fitted velocity. (c) Scaled turbine in study. Note the reference turbine has similar Reynolds number in water as well as air. The only difference in Reynolds number for the scaled model is the diameter.

2.6 Acoustic doppler velocimeter (ADV)

For measuring flow velocities there are several methods to choose from, one of which is acoustic sensors. In this study, an acoustic doppler velocimeter (ADV) from Nortek called Vectrino+ is used. The sensor consists of one transmitter and four receiver arms as depicted in Figure 2-7. It records data by sending out an acoustic pulse through the transmitter and picking up the echo in the four receiver elements. The emitted pulse has a constant frequency, while the received echo experiences a change in frequency. By finding the doppler effect (change of frequency), a velocity vector is then recorded onto a computer as it is proportional to the registered change. Data collection rates for the Vectrino+ can reach upwards of 200Hz as opposed to the standard 25Hz Vectrino. [23]

An issue concerning the use of acoustic sensors is getting a reading in water because the emitted pulse cannot reflect from the water itself. There need to be small particles in the recorded environment, to receive an echo. For a water tank experiment, the solution is to evenly distribute particles in the water, so called seeding. There is also a need for good mixing in the pool before conducting the experiment. This makes sure the particles are scattered in the entire depth of the pool and not just at the bottom.

Figure 2-7: Vectrino ADV from Nortek

3 Methodology

The experiment is carried out using actuator discs as displayed in Figure 3-1. Both single- and multi-rotor setups are analysed in a towing tank using an ADV to record the data. The single-rotor analysis was used as a point of reference to compare against the multi-rotor setup. The discs are arranged in a four- and seven-disc setup which can be viewed in Figure 3-1. For simplicity reasons, the discs are non-rotating at fixed positions.

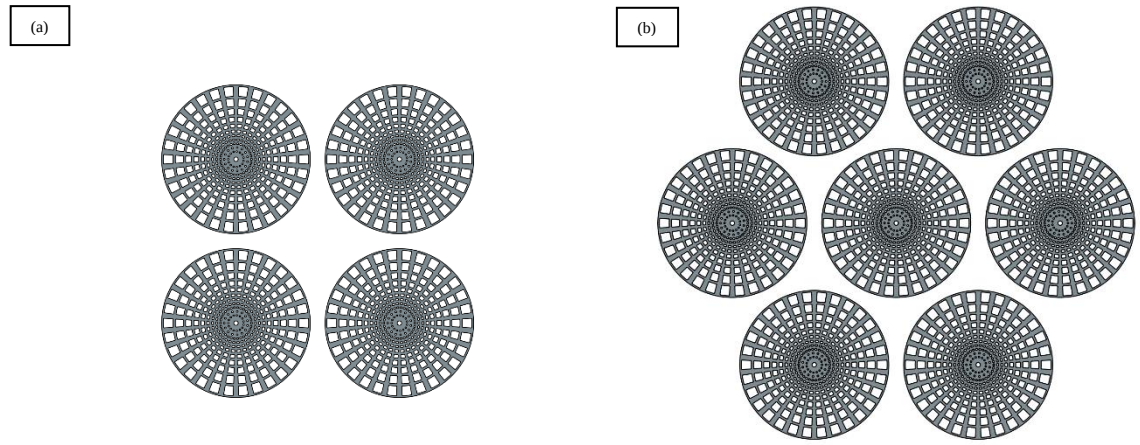

Figure 3-1: (a) MR4 with spacing 0.1D (b) MR7 with spacing 0.1D.

3.1 Marin Lab

The tank used for the experiments measured 50 meters in length, 3 meters in width and 2,2 meters in depth. Two towing carriages are used to mount and drag the discs and ADV through the water. They can move in both directions and run at controlled velocities. The carriage and complete lab setup are displayed in Figure 3-2 (a) and (b).

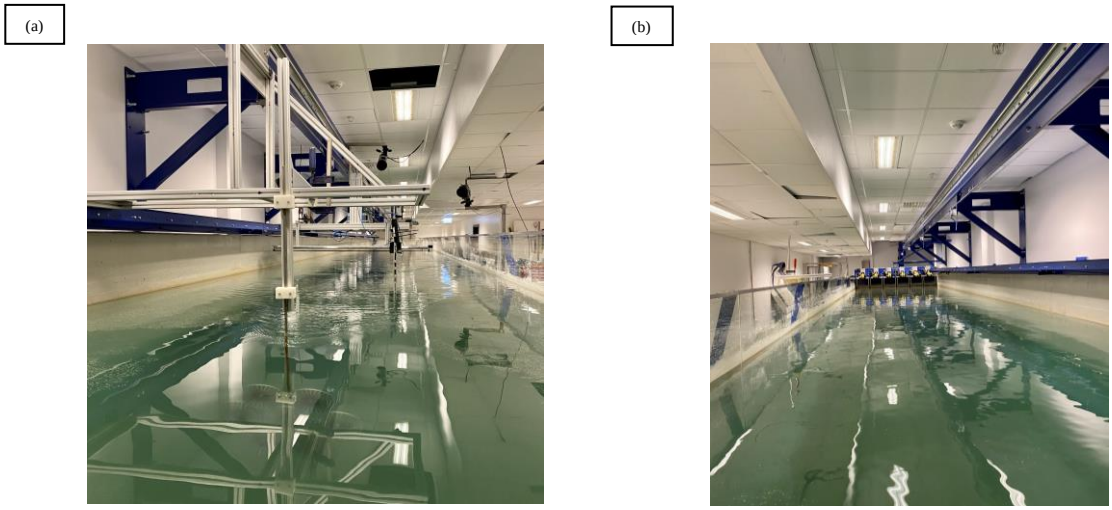

Figure 3-2: (a) Rotors are positioned in front of a small carriage, while the ADV sits in the back at the main carriage. (b) Wave generator in the end of the pool.

For this experiment, the carriages moved with a velocity of 0.4 m/s. Low speed was used to prevent stern wave production, which could disturb the readings of the ADV. Bending of the structure would also occur at too high velocities. A multi-rotor drag study from Hansen et al

[12] with the same disc setup, found that the effect of flow velocity was insignificant above a certain level. Increasing the incoming velocity would therefore only lead to more bending of the structure and potentially jeopardize both the structure and the results. Bending is a rotation of the pitch axis and could lead to an unwanted deflection of the wake flow.

Incoming turbulence and shear could have been produced in the towing tank by using a grid but was however ruled out of this experiment. The incoming turbulence was therefore estimated to be 0% when long enough waiting times were implemented between the runs of the carriage. For future experiments, turbulence can be produced to see how turbulent inflow conditions affect the wake recovery. Seeding powder is utilized in the water tank to obtain data and has been distributed by hand in previous experiments. A wave generator pictured in Figure 3-2 (b) was used in combination with manual stirring to get appropriate mixing of seeding in the tank before the experiment. Particles tended to float to the surface or sink to the bottom of the tank. It was therefore important to have a thorough mixing process before data collection started. Test runs were carried out until the readings reached desirable signal to noise ratio. Under the experiment, the discs produced enough mixing on their own. Further stirring was therefore only necessary in-between downtime or breaks.

3.2 Structure

The multi-rotor structure consisted of three main parts: discs, staffs, and joints. While the discs were laser cut from a standardised model the joints were 3D printed from our own design, which can be viewed in Figure 3-3. Several prints were tested to find suitable dimensions and settings. Utilising 3D-printed plastics for joints gives a cost benefit, but at the expense of strength. Meaning the size is bigger to withstand forces. Even so, the effect on the results is probably minimal due to the limited flow in the centre. Discs were mounted on the joints using screws and nuts ensuring its firmly mounted, and staffs were used between all joints to assemble the multi-rotor. There is also a staff going from the centre of the multi-rotor connecting to the towing carriage. Figure 3-4 displays the complete setups.

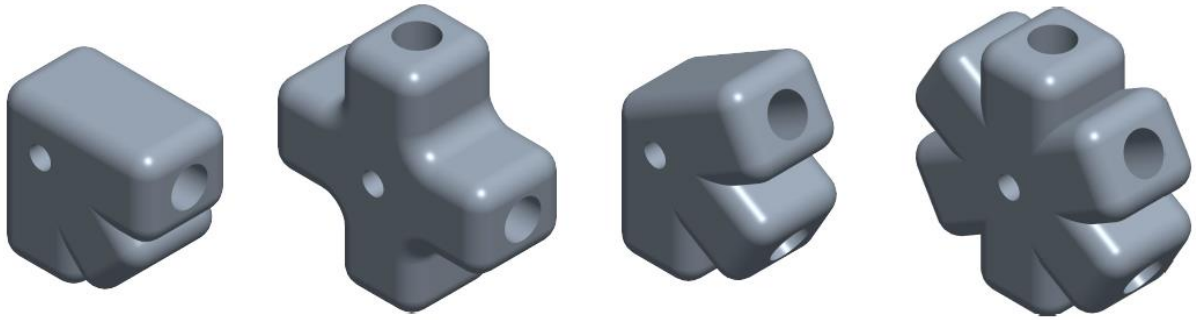

Figure 3-3: CAD models for MR4 and MR7 joints

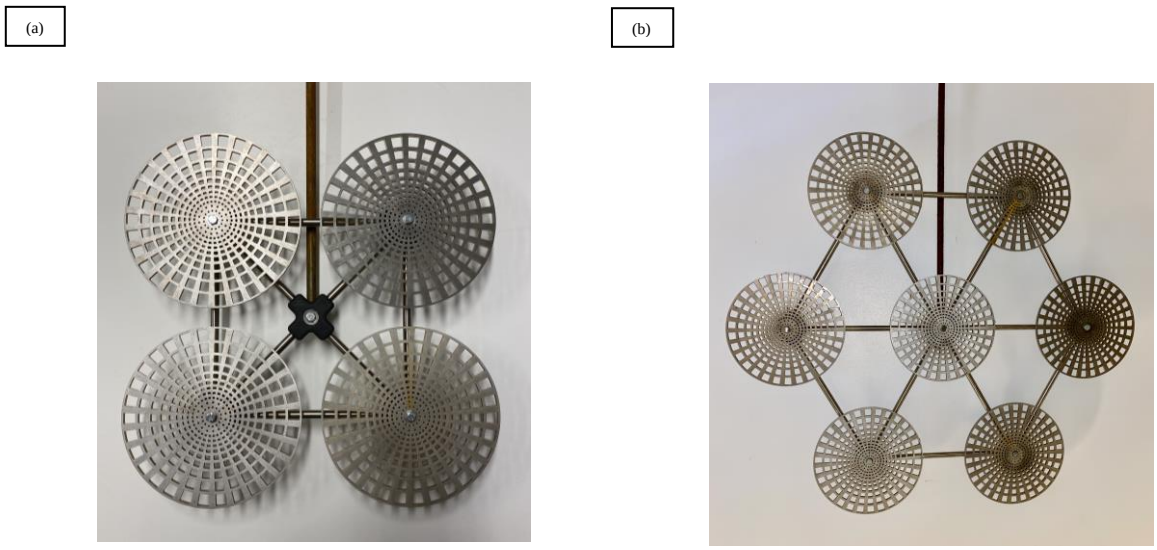

Figure 3-4: Complete setup of (a) MR4 0.1D (b) MR7 0.4D.

3.3 Measures

Wake flow measurements were carried out parallel to the disc. It has been measured at different downstream locations displayed in Figure 3-5, with a constant yaw angle of zero (γ=0°). Each location provides one wake profile consisting of numerous data points. Since there are more changes in the near wake of the turbine, data collection was chosen to be higher than for the far wake recordings.

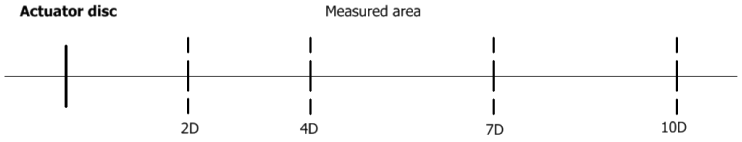

Figure 3-5: Downstream locations.

All wake measurements have been recorded in the centre of the turbines as shown in Figure 3-6. But to minimise the experiment time, the multi-rotors have more data points from left to centre than from centre to right. Since the geometries are symmetric, readings should also be symmetric around the vertical centre axis. The right-hand side therefore only has half the number of data points relative to the left side.

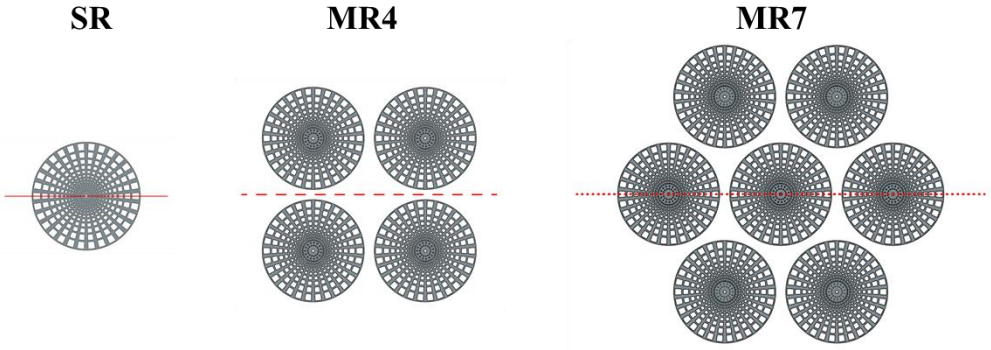

Figure 3-6: Pictorial legend of parallel wake measurements.

In addition to parallel wake flow, a centreline has been recorded perpendicular to the disc in the streamwise direction for the multi-rotors. It stretches from -1D to 10D, with only a small gap around 0D. This gives a better view of how the flow and turbulence develop from start to end, since the wake profile has only been performed at certain locations. However, it does not give much information about the sides. The two is therefore more valuable combined than each separately. For the single-rotor, measurements from previous studies are being used and thus only ranges from -1D to 6D. Although, one point is plotted at 10D by using data from the wake profiles. Since there are few sudden changes in the far wake, this gives a sufficient picture of how the flow develops.

Because of jet streams and blockage effect, the recorded data may differ substantially in the near wake area through the cross-section. The MR4 is therefore measured at both turbine centre (TC) and offset centre (OC) from -1D to 4D. Measurement in the far wake was suspected to be similar between TC and OC and was therefore limited to only TC. All centreline measuring points can be viewed in Figure 3-8.

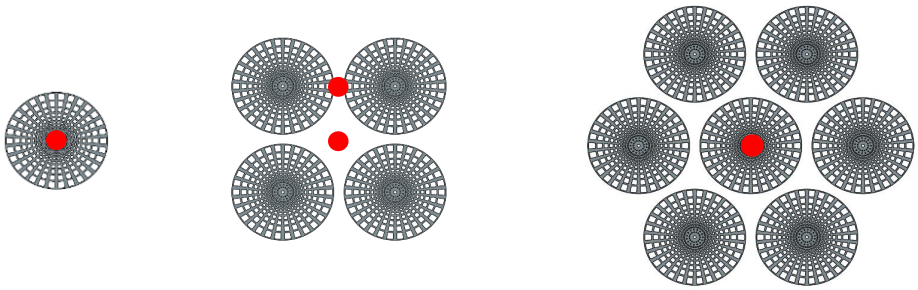

Figure 3-8: Pictorial legend of perpendicular centreline measurements.

When defining spacing and other points of measure, the terms y/D and x/D have been used to compare different disc setups by making them dimensionless. Depending on the type of setup and measures, different approaches have been used to define diameter. For the single-rotor, it is straight forward a diameter of 20 cm. The tricky part is defining the multi-rotors when they all have different spacings and geometries of squares and hexagons. First off, the diameter used for distances in the wake was set to be the number of discs in width. For MR4 this would mean two discs with a total diameter of 40 cm, and for MR7 it would be three discs with a total of 60cm. by using this definition, it is independent of rotor spacing. Meaning the same diameter applies to all MR7 turbines, even though they have different distances between the discs. When defining rotor spacing, the diameter of a single-rotor has been used instead of the total setup diameter. 0.1D spacing therefore corresponds to 2 cm. These definitions are illustrated in Figure 3-7.

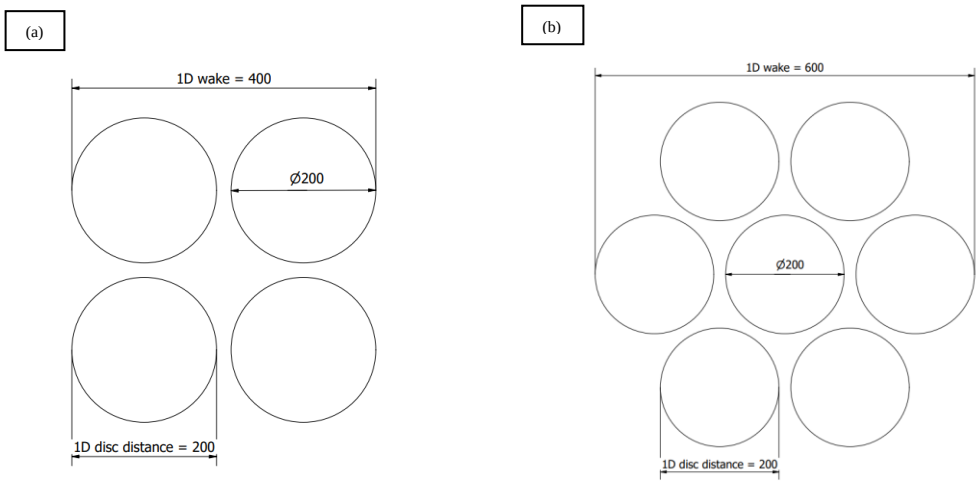

Figure 3-7: Definition of diameter and spacing for (a) MR4. (b) MR7.

3.4 Sources of error

Several elements can contribute to inaccuracies and sources of error in the measured data. It is normal to section these uncertainties into two main groups, systematic and random error. The former generally refers to consistent errors related to the measuring device or other invariable errors. Common examples include a faulty device, lack of calibration, and observational error. Repeating an experiment would accordingly so yield the same margin of error every time and could therefore be adjusted for in the results if noticed. Random error or precision error is on the other hand unpredictable and cannot be replicated. By repeating an experiment, the outcome would change each time. Typically, these errors appear when changing procedures, reaching limitations of devices, or mounting imprecisely in an uncontrollable manner.

3.4.1 Random error

Rigging of equipment is mostly done by hand in this experiment and would therefore be the main contributor to error. The carriages and traverse mechanism for ADV are computer-controlled and can run at regulated velocities and positions, but the distance between the carriages needs to be set manually. For each wake profile (2D, 4D, 7D, 10D) the carriages need to be moved to have the correct distance between the discs and ADV. A Measuring tape and reference points were used to calculate the distance. Because of the measuring inaccuracy, the true distance of the wake profile could be at 1.98D instead of 2D and hence being a random error. For future experiments, a laser meter would be a better solution. Furthermore, the ADV needs to be installed at 0° angle but is mounted on eyesight, as there is currently no available control mechanism in the lab. Nevertheless, large deviations are discovered in the test runs and corrected. It is therefore only a minor issue. The angle of the mounted turbines is similarly something that affects the readings and can be noticed in the results, but the exact angle and how much it affects the wake is hard to say. The height of the ADV is set using a meter stick, which is believed to be ± 1 cm off. However, it is not possible to find the exact error and can neither be accounted for in the results.

Low mixing produces large amounts of noise in the readings and can therefore be a big contributor to error, due to its effect on the mean value and standard deviation. The precision also varies at all times because of moving particles. Meaning that even with good mixing the result changes for each run. A measurement performed with the same equipment was therefore conducted in the Marin lab by Bjørnsen [24], to find the precision of the ADV. The margin of error was after a series of test runs found to be 1.76%.

3.4.2 Systematic error

It also becomes visible in the wake results when the ADV is not perfectly aligned with the discs, as the result becomes shifted towards either side. This is luckily something that can be adjusted for when processing the results. There is in addition always a chance that the ADV is not calibrated correctly. Systematic errors also include possible mistakes made when processing the data with filters and other calculating measures.

3.5 Data processing

All ADV readings are converted and imported into Matlab for data processing. To ensure good quality, filters are applied. Firstly, a Hampel filter is used to remove noise from the readings. By choosing a sample and calculating the standard deviation, all data above 2,4 times the standard deviation can be removed. Secondly, the start and the end of the recording are cut out. This is because the probe experiences acceleration and disturbed readings at these points. Figure 3-9 is a visual representation of the applied filters from one of the recordings.

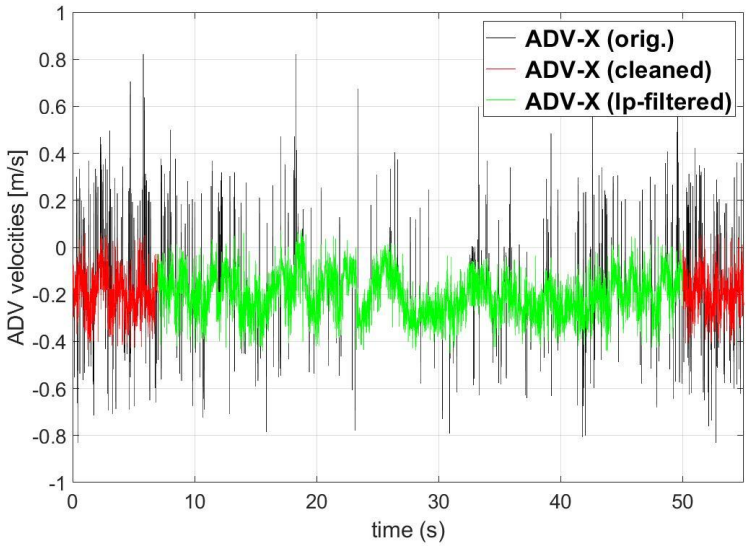

Figure 3-9: Data filters used for readings. Black lines are original recordings, red is Hampel filter and green is the final dataset using cut-out.

4 Results

The following chapter includes a detailed evaluation of the lab experimental results. Wake profiles for SR, MR4 and MR7 are compared and analysed at different downstream distances. The selected setups are also evaluated using recorded centre streamlines, to see the change in turbulence and velocity deficits through the wake. For the MR4 turbine, an offset streamline has also been recorded to investigate the influence of the measurement location. In addition, various distances between the MR7 discs are studied to find the effect of rotor spacing.

In the results, the average velocity deficit Δu_{mean} is divided by the freestream velocity u_0, and the cross-sectional length y is divided by the diameter of each rotor setup. This gives a dimensionless relation of diameter and velocity in the wake. Hence the different wake profiles and streamlines are comparable regardless of size and incoming flow. The non-dimensional turbulent kinetic energy is defined as tke/u_0^2. Turbulence intensity is included in the results but will not be mentioned, since it is less accurate than turbulent kinetic energy. It is only included in the results for comparison with other articles.

4.1 SR and MR wake comparison

This section includes a comparison of the cross-sectional wake profiles for the three different rotor setups. The results are presented in Figure 4-1 with a spacing of 0.1D for MR4 and MR7. Downstream distances include 2D and 4D as near wake and 7D and 10D as far wake. In this project, the single-rotor have not been recorded at 7D and therefore only contains the multi-rotors. Both normalised velocity deficits and their respective turbulence profiles are depicted for turbulent kinetic energy and turbulence intensity. The black vertical line in the figures represents the area of the rotors.

At 2D both multi-rotors have an equally lower velocity deficit than the single-rotor, reaching around 70% in contrary to 100%. This might be due to jet streams between the single discs as mentioned in chapter 2.2, leading to higher turbulence at earlier stages of the wake. MR4 shows a lower velocity drop at the middle of the rotor as opposed to the single-rotor and MR7, which is most likely due to the centre opening. While MR4 may experience jet streams in the middle, the single-rotor and MR7 have a disc blocking the flow. Looking at the turbulence, all profiles peak at the turbine sides where free stream flow is faced, but the MR4 also has a local peak in the centre due to its open space.

Further downstream at 4D all wakes are sharing a Gaussian shape. MR7 has regenerated slightly more than MR4 at 45% and 50%, respectively. But although the single-rotor is still at 60%, it recovered 40% of its deficit in only two diameters. This could be explained by the turbulent kinetic energy being higher at 2D and 4D than for the compared multi-rotors. It supports the theory that higher turbulence gives faster recovery. It is also worth noting that all curves have a more uniform shape, proving the wakes are well mixed at this downstream distance.

At 10D the wake profiles are more alike. Single-rotor has recovered the most, having a velocity deficit of 15% compared to both multi-rotors at 20%. Turbulence is also lower for the single-rotor turbine. Their shapes are all similar and more widespread, with no distinct peaks. This is

because of an expansion of the wake due to mixing with freestream flow in the regions at y/D=±0.5. The turbulence and velocity deficits are therefore more evenly distributed along the cross-section. Overall, the major differences between the setups can be found in the near wake, where the geometry play a key role in turbulence, mixing and velocity deficits.

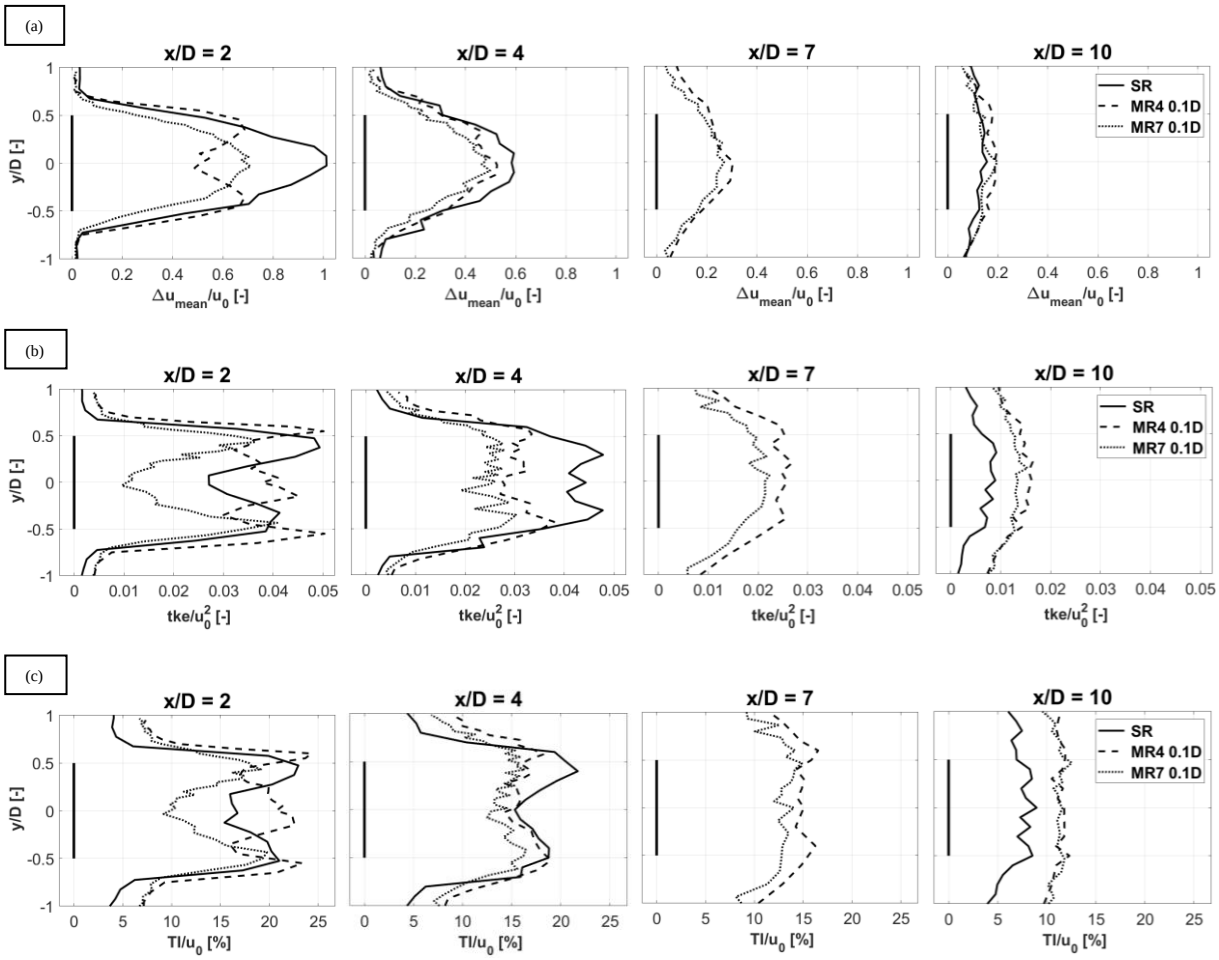

Figure 4-1: Wake profiles for SR, MR4 and MR7 with 0.1D spacing, showing: (a) Normalised velocity deficits $\Delta\bar{u}/u_o$. (b) Normalised turbulent kinetic energy tke/u_0^2. (c) Turbulence intensity.

To see continuity in how the wakes develop, a centreline measurement is shown in Figure 4-3. It ranges from -2D to 10D and thereby recording both upstream and downstream from the turbine. The single-rotor is due to limited data only ranging from -2D to 6D. Upstream of the rotor setups all curves experience an increasing loss towards the rotor, although slightly higher for the single-rotor. This was as expected a result of blockage and is illustrated in the 1D momentum theory Figure 2-2. Downstream of the rotor there is on the other hand some distinct differences. All curves seem to meet at around 4D even though they have different paths. But while the single-rotor and MR7 start on top and decreases, MR4 starts on the bottom and increases. This is most likely because of its opening in the turbine centre. The fact that the deficit is lower right behind than upstream of the rotor, may indicate a jet stream.

MR7 sees its biggest decline right behind the rotor and slowly evens out, whereas the single-rotor gradually drops and reaches an inflexion point at roughly 3D. At the same time, MR4 has a global maximum at this downstream region. After 4D the velocity regeneration follows a similar path for all disc setups. Even though the single-rotor is lacking data from 6D-10D, it is

unlikely that there are any abrupt changes. This can be seen in the point measured at 10D behind the single-rotor.

The three setups have greatly different turbulence plots because of their associated geometry. In the near wake of the rotor, there are complex flow patterns because of jet streams, blockage, shear gradients and mixing. This especially counts for the multi-rotors. It is therefore difficult to analyse and justify the findings based on only these results, but an attempt is made.

The single-rotor wake experiences constant turbulence from 0D-2D at its centreline, before inclining heavily towards 4D. It is reasonable to believe that the centreline is unaffected by the free-stream flow up until 2D, and therefrom being increasingly influenced by the shear gradients. The constant turbulence is therefore generated by only the disc itself. Up to about 3.5D is recognised as the turbulence production region where the turbulent kinetic energy peaks. At this point, the high mixing ensures decaying and decreasing turbulence levels. Comparing against the wake profile in Figure 4-1 (b), the statement makes sense considering there is a lot more turbulence on the sides at 2D which progressively becomes more uniform towards 4D, in what becomes the turbulence decay region.

MR4 is a different matter since the wake centre is in an unblocked path. There is no disc standing in the way of the flow. As a result, vortices shed from the single disc's edges cause high turbulence at the start of the wake before rapidly declining to 1D. At this point, the centre is gradually affected by the free stream flow just like the single-rotor. It therefore reaches a new turning point at 2D before being reduced again. Some of these indications can also be found in Figure 4-1 (b). In contrast to the single-rotor, MR4 has three points of maxima instead of two at 2D. This indicates two sources of turbulence production. One in the centre and one around the rotor's edges. For this reason, MR4 has two major peaks in Figure 4-3 (b) as opposed to the single-rotor's one. The following explanation is illustrated in Figure 4-2 for all disc setups.

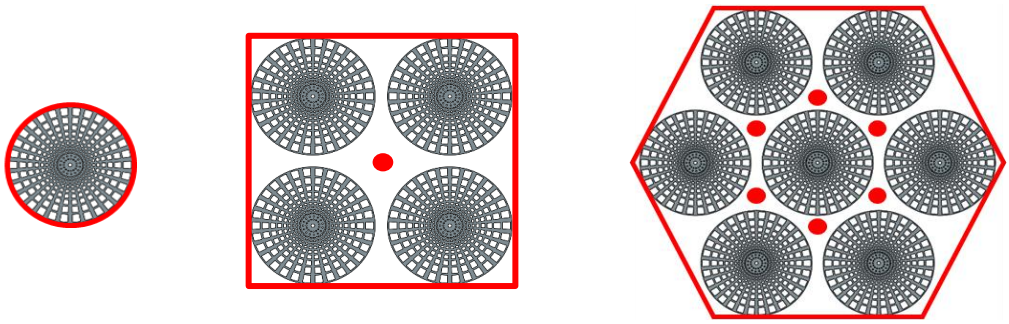

Figure 4-2: Illustration picturing possible sources of turbulence production for SR, MR4 and MR7. Red dots are jet streams, and red lines are shear gradients due to free stream flow.

Plots for MR7 are in some ways a combination of MR4 and single-rotor. The disc in the centre prevents high turbulence from start, but the surrounding flow quickly influences the centrelines. This leads to the first turning point at 1D. The big difference is in this case, that the surrounding flow primarily comes from six enclosing jet streams and not the free stream flow like it would on the single-rotor. Further on, turbulence decline until past 2D before starting a new ascend towards 4D. This climb is on the other hand, mainly due to the shear layer separating the discs from free stream flow. Once at the top, turbulence slowly starts to decay.

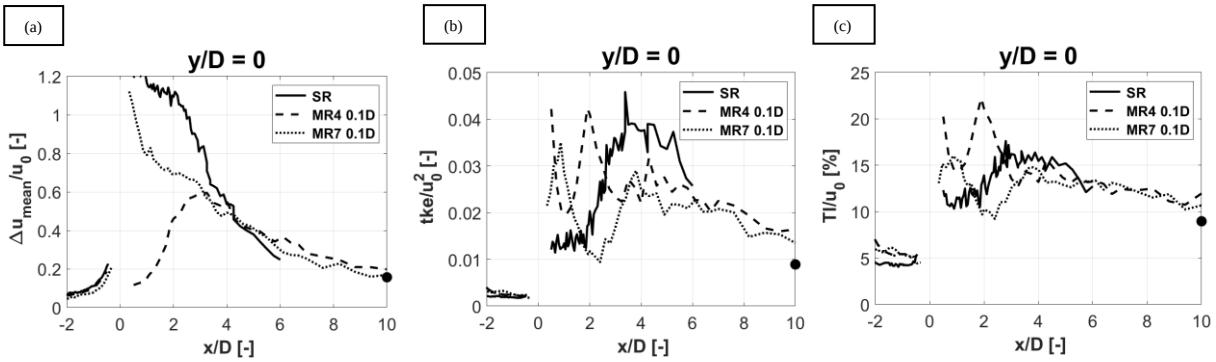

Figure 4-3: Centreline profile for SR, MR4 and MR7 with 0.1D spacing showing: (a) Normalised velocity deficits $\Delta\bar{u}/u_o$. (b) Normalised turbulent kinetic energy tke/u_0^2. (c) Turbulence intensity. Note: black dot illustrates single-rotor values at 10D taken from wake measurements.

4.2 MR7 with different inter-rotor spacing

Wake profiles for MR7 are measured with different inter-rotor spacing at 0D, 0.1D and 0.4D. The results are presented in Figure 4-4 and show normalised velocity deficit ($\Delta\bar{u}/u_o$) and normalised turbulent kinetic energy (tke/u_0^2). There is also conducted centreline measures for the different MR7 setups to see how spacing affects the wake. This is presented in Figure 4-5.

There is a significant variation in the wake for the different setups at 2D downstream. The turbine with 0.4D spacing has recovered the most at this point, with a velocity deficit of approximately 40%. In contrast, the multi-rotor with no spacing has barely regained any velocity, while 0.1D is at 70% of the freestream velocity. This implies that an increase in spacing leads to better mixing in the near wake region.

At a downstream distance of 4D, the velocity plots are already more alike. The 0.4D turbine still has the lowest velocity deficit, but 0.0D and 0.1D are not far apart. At this point the turbulence is significantly lower for the turbine with 0.4D spacing, meaning it has already experienced good mixing. For the other setups, the turbulent kinetic energy experiences a lot of variation throughout the cross-section at 4D, which is typical for the transition region of the wake. This fluctuation in combination with high levels of turbulence makes the velocity regenerate faster. The rate of velocity recovery is therefore larger for the multi-rotors with 0.1D and 0.0D spacing at this downstream distance. Which could imply that the transition region comes earlier with more spacing.

In the far wake region at 7D and 10D, the wakes are at an almost equal level. There is only a slight difference in the turbulence plot. The wake profile for the multi-rotor with 0.0D spacing should behave almost like the single-rotor wake, with the difference being small jet streams in the intersections of the discs.

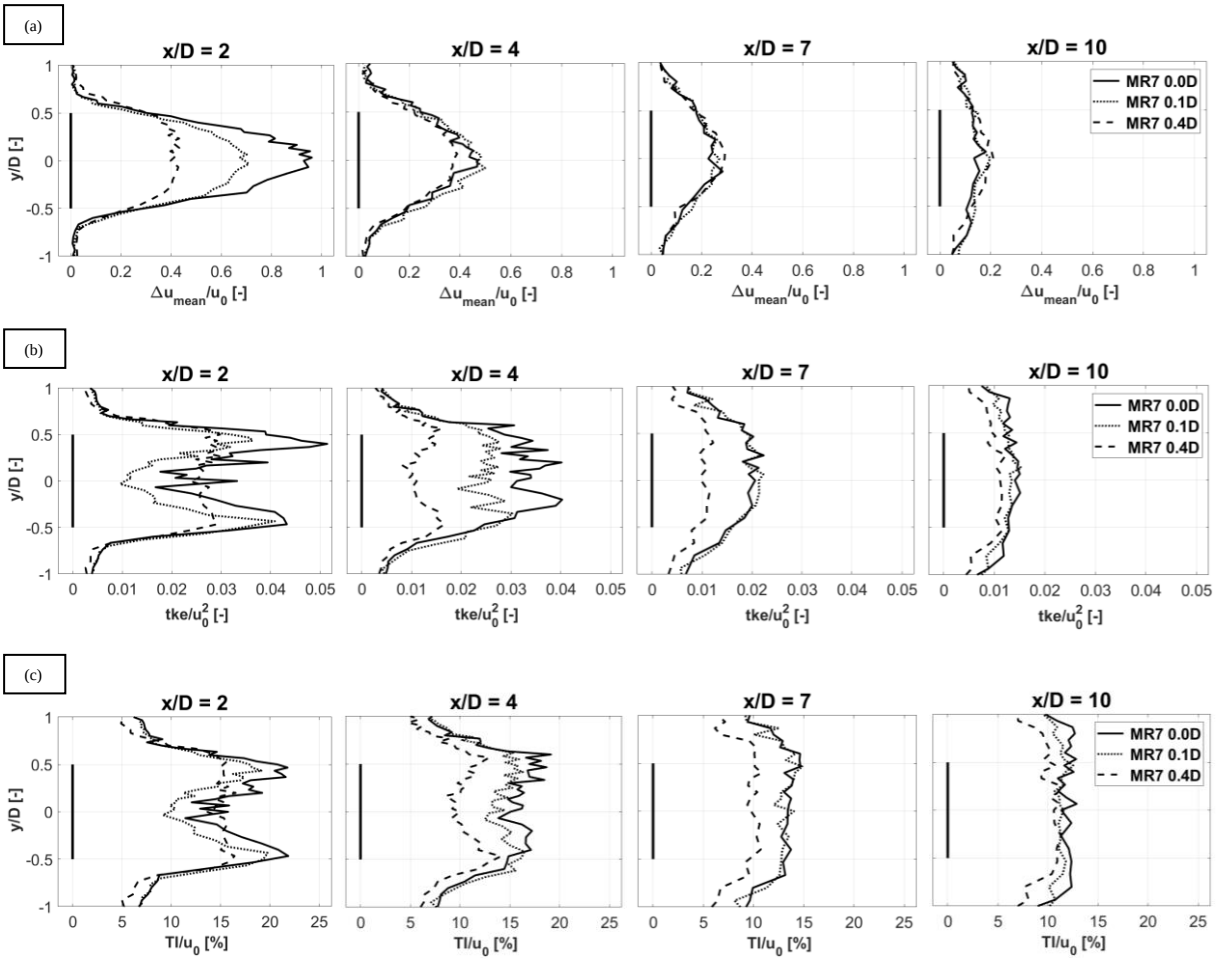

Figure 4-4: Wake profiles for MR7 with 0.0D, 0.1D and 0.4D spacing, showing: (a) Normalised velocity deficits $\Delta\bar{u}/u_o$. (b) Normalised turbulent kinetic energy tke/u_0^2. (c) Turbulence intensity.

In Figure 4-5 (b) the turbine with 0.4D spacing shows a high level of turbulent kinetic energy behind the turbine before it flattens out at 2D-3D downstream. This is also seen in the velocity deficit curve, with a steep change up to about 2D. At later downstream stages it does not peak again as the other multi-rotor setups. This could be because of the distance from the centre to the outside freestream, or because the mixing is extremely high behind the turbine.

The curve with no spacing experiences a peak in turbulent kinetic energy at about 0.5D, which might be due to mixing from the jet streams around the disc in the middle. Further downstream it has an increase at 2D, perhaps because of shear gradients from the free stream flow. This gives a smoother curve for the velocity deficit, but it does not reach the same level as the turbine with 0.4D spacing until 5D downstream. When it comes to the turbine with 0.1D spacing it is quite similar to the one with no spacing, but the velocity recovers faster in the start due to bigger jet streams. Because of an increased distance from the turbine centre to the outside of the turbine, it takes longer time before outside shear gradients are noticed in the measures. It therefore reaches the second peak at a later stage than for 0.0D spacing. After 4D there is less difference for the velocity deficit in the three plots. At a downstream distance of 10D, the turbines have recovered to about 20% of incoming velocity.

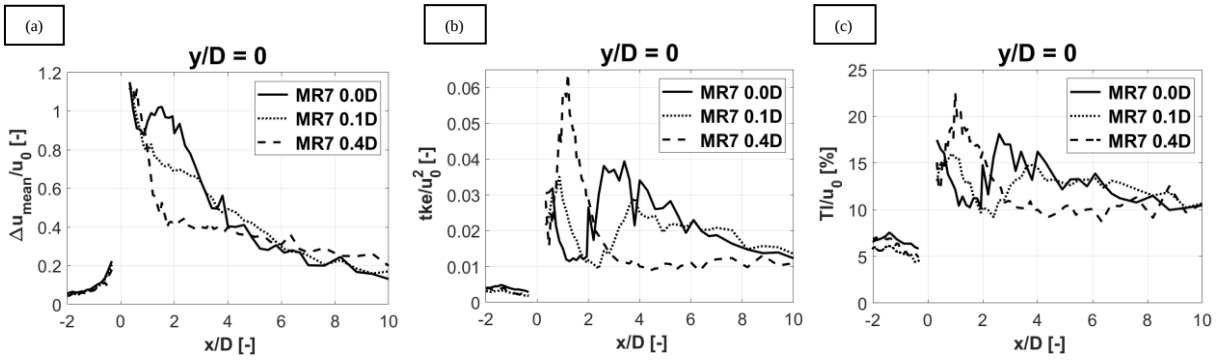

Figure 4-5: Centreline profile for MR7 with 0.0D, 0.1D and 0.4D spacing, showing: (a) Normalised velocity deficits $\Delta\bar{u}/u_o$. (b) Normalised turbulent kinetic energy tke/u_0^2. (c) Turbulence intensity.

When comparing the MR7 with 0.0D spacing against the single-rotor in Figure 4-6, the multi-rotor is almost equal to the single-rotor. Both velocity deficit and turbulence follow a similar path. There are only small differences between the two, for example in the near wake between 0D-1D. Otherwise, they decline and increase in the same places, although not always at the same values. The multi-rotor therefore almost acts as one big single-rotor. When comparing to 0.4D it proves just how much impact the spacing can have.

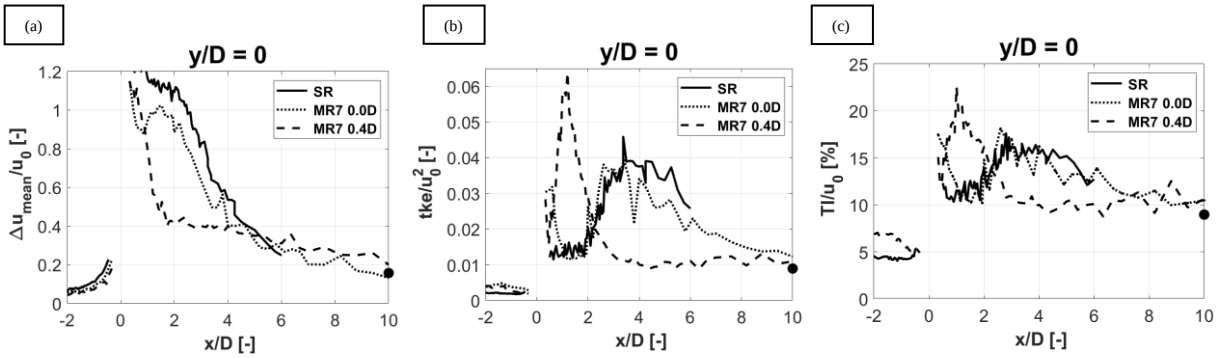

Figure 4-6: Centreline profile for SR and MR7 with 0.0D and 0.4D spacing showing: (a) Normalised velocity deficits $\Delta\bar{u}/u_o$. (b) Normalised turbulent kinetic energy tke/u_0^2. (c) Turbulence intensity. Note: black dot illustrates single-rotor values at 10D taken from wake measurements.

4.3 MR4 offset measurement

Since both the single-rotor and MR7 unlike MR4 have a disc in the centre, the centreline readings are quite different. Therefore, to better understand the result and how the measuring location affects the readings, an offset measurement was performed for the MR4 turbine. By placing the probe between the two upper discs, the readings would not be too affected by the centre jet stream. Seeing that the substantial changes happen in the near wake, recordings were limited to x/D=4. The results are presented in Figure 4-7.

Upstream of the turbine there are barely any noticeable changes, neither for velocity deficit nor turbulence. Downstream of the turbine is where it starts to differ. In Figure 4-7 (a) the offset trajectory is steeper and starts at a higher point. Accordingly, it peaks at an earlier and higher stage. In comparison, the turbine centre is somewhat delayed. Nevertheless, they both make sense in context with previous measurements from SR, MR4 and MR7 in Figure 4-1. At 2D the offset centre curve peaks just below 0.7 while the turbine centre is approximately 0.5. These

are the same values found in Figure 4-1 (a), with the only difference being horizontal readings instead of vertical. This is logical, seeing that if measured correctly, there should not be any differences between horizontal and vertical. Bearing that in mind, stern waves and global blockage are to an extent proven not to affect the wake in this study. Meaning the parameters of size and velocity was reasonable set. After 3D, the two trajectories almost merge in Figure 4-7 (a) and thereby showing that there are small differences between them.

The turbulence in Figure 4-7 (b) has some major differences between the curves. While the offset centre (OC) is more constant with only small abrupt changes, the turbine centre (TC) is highly fluctuating. A plausible reason for this is that OC gets influenced by both the free stream flow from the outside and the jet stream in the centre at the same time. Therefore, it experiences high constant turbulence instead of intervals like TC. Both curves start to decline after 2D, and just like the velocity they follow each other's trajectories. There is no reason to believe this change further downstream, as the wake turbulence becomes more and more isotropic in the far wake.

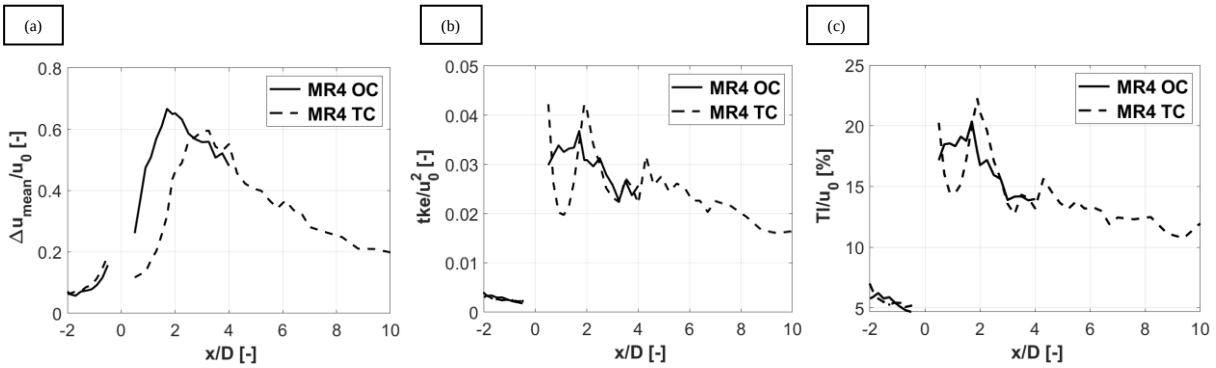

Figure 4-7: Centreline profile for MR4 at turbine centre (TC) and offset centre (OC), showing: (a) Normalised velocity deficits $\Delta\bar{u}/u_o$. (b) Normalised turbulent kinetic energy tke/u_0^2. (c) Turbulence intensity.

5 Discussion

This section includes different results from literature compared against the lab experimental data. The main source for this comparison is LES performed by Bastankhah et al. [10] on a rotating actuator disc model, for different multi-rotor setups. Their simulations are done with an incoming turbulence intensity of 6.7%, and with a wall shear stress according to standard log law. The results compared are wake measurements for SR, MR4, and MR7 with a spacing of 0.1D, and centrelines for the respective setups. In addition, the effect of inter-rotor spacing is included in the discussion. Here, MR7 from our experiment is studied in correlation with MR4 from Bastankhah et al. for different spacing setups.

5.1 Effect of rotor number

For the single-rotor at 2D downstream, Bastankhah et al. obtained a velocity deficit of 60% in the simulations pictured with a solid line in Figure 5-1 (a). Our results from Figure 4-1 (a) show a velocity deficit of 100% in the centre, which is a considerable difference. It is worth mentioning that the simulation contains two deficit peaks instead of one, which is probably because of a non-uniform axial force distribution over the radius. For a disc, the blockage is highest in the centre of the rotor but for a real turbine, the velocity deficit is slightly lower in the centre. This is because it extracts less energy in this area. Given that Bastankhah et al. operates with generated force fields, and does not simulate an actual CAD drawn disc, it makes sense that they have two deficit peaks. Further downstream at 4D the deficit inequality is almost evened out with simulations having a deficit of 55% as opposed to the experiment showing 60%. These variations are also observed in the centreline measurements from Figure 5-2 but results from the lab in Figure 4-3 (a) are in addition showing negative velocity right downstream of the disc. In the turbulence intensity graphs depicted in Figure 5-1 (b), the shapes of the curves are very much alike our results from Figure 4-1 (c). Although, the intensity levels are vastly different. This is probably because of a significantly higher inlet turbulence in the simulations. Since the lab experiment does not operate with inflow turbulence, added streamwise turbulence intensity is the same as total. While in the simulations, the inlet is subtracted from the total. If comparing both results for total turbulence intensity, the single-rotor has a value of around 19% in the simulations when adding the 6.7%. Whereas in the lab results it reaches its highest point of around 23% at 2D downstream. The difference is therefore not that distinct after all. When looking at 4D, this dissimilarity is almost non-existent. Despite the simulations actually having an increased turbulence at this point, they both end up at around 22% peak and 16% in the centre. However, at 10D the differences have increased, yielding higher turbulence for the simulation. The course of action follows two contrasting flows. While our experiment starts high and slowly decreases by the distance, the simulation has a more or less constant turbulence development. This could be due to the inlet turbulence, or other chosen parameters.

MR4 wake profiles for simulations and experiment have similar shapes throughout the different downstream distances. But there is a considerable difference for the velocity deficit in the near wake region. While simulations at 2D downstream in Figure 5-1 (a) peak at 30%, data from the lab has a velocity deficit of almost 70% in Figure 4-1 (a). The velocity regeneration at the next downstream distance of 4D is a few per cent for the simulations, whereas empirical data only

show 20%. A distinct difference between the curves is the velocity in the middle of the turbine. Although they look similar in shape, the simulated data has a far bigger drop in the centre. It only reduces by around 5% at 2D, compared to 50% for the experiment. Also, the wake barely regenerates downstream. Instead, the deficit in the centre increases, making the total deficit more uniform. This stands in contrast to the experiment where the total deficit decreases as well as becoming uniform. Further downstream at 7D the velocity deficit differences are even less. Once again, the simulations barely regain anything, while the experiment takes another 20%. At this point, there is only around 5% separating the two as they have respectively 25% and 30% in velocity deficits. This equalizes at 10D, where they both end up at 20%. The compared centrelines in Figure 5-2 and Figure 4-3 (a) are also quite equal in shape, but the simulation has both a lower and shifted peak. While the experimental results peaks around 3D with a velocity deficit of 60%, simulation has its lowest velocity in the transition region about 5D and 30%. For the turbulence intensity, changes are minimal throughout the distances for the simulated results. Both shape and intensity have small variations downstream in Figure 5-1 (b). It does slowly decrease and alter into a uniform shape, but the changes are minimal when comparing against the experimental data. The shape of the curve seems almost regenerated when looking at 2D downstream because the top and bottom is only separated by a few per cent. Unlike the measured data in Figure 4-1 (c) where the gap is quite distinct. It also contains a total of four peaks as opposed to the measured three. Instead of having a considerable turbulence stream in the middle, it distinguishes between the centre and start of the discs. Although, when looking closely at the experimental results, the centre peak is in fact shifted a bit downwards. This could implicate that our results are missing one peak due to lack of data, considering more data points were collected on one side than the other.

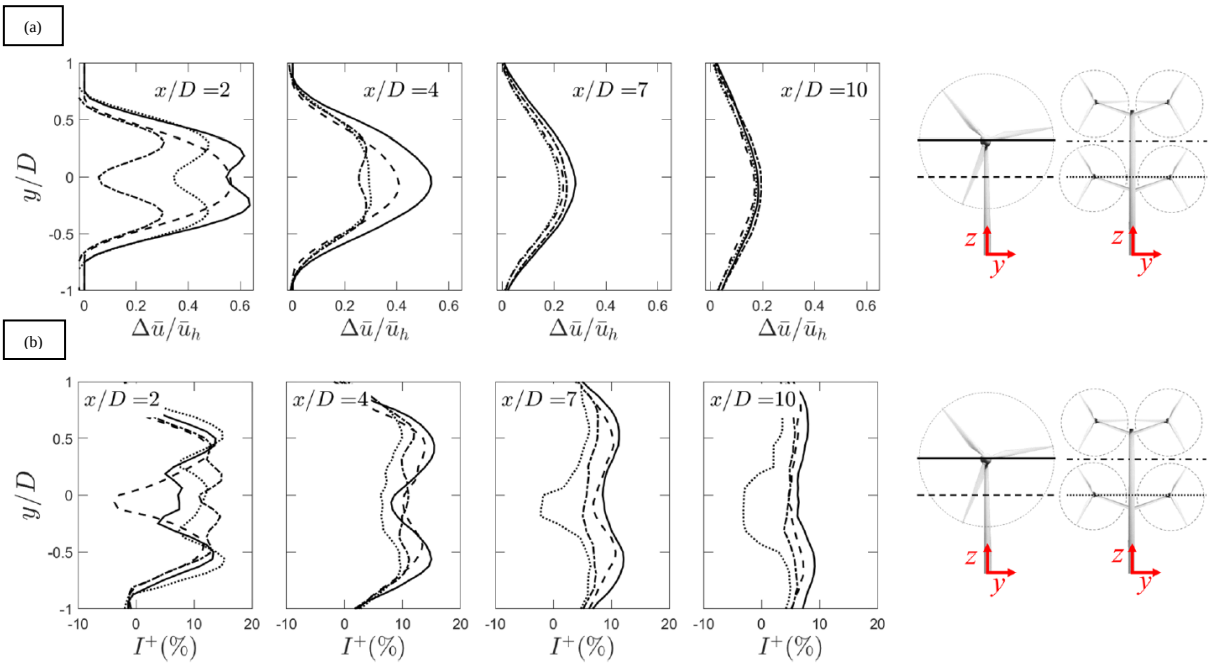

Figure 5-1: Single-rotor and MR4 wake simulation from Bastankhah et al. (2019) showing: (a) Normalised velocity deficit. (b) Added streamwise turbulence intensity.

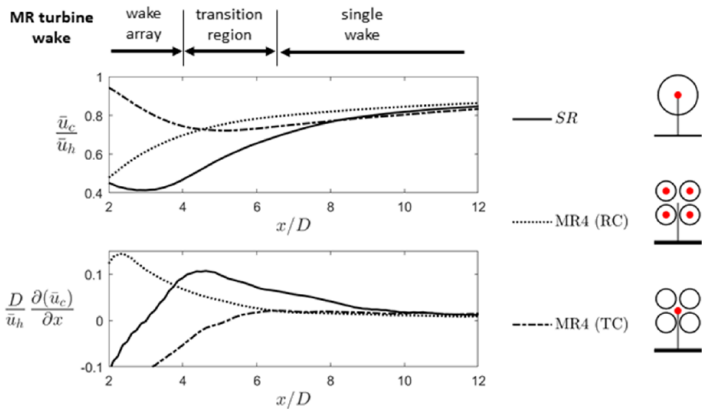

FIG. 6. Variation of the normalized streamwise wake center velocity (*top*) and its derivative (*bottom*) with the streamwise distance. For the MR4 turbine, RC denotes the streamwise velocity downwind of the rotor center (averaged of four rotors), while TC represents the velocity downwind of the turbine center with (y, z) equal to (0, z_h).

Figure 5-2: Single-rotor and MR4 centreline measurement from Bastankhah et al. (2019)

For MR7 at a downstream distance of 2D, there is measured a velocity deficit of 45% in the simulations given in Figure 5-3. On the other hand, the experimental results show an almost 70% decrease in velocity at the same downstream distance in Figure 4-1 (a). Their shapes are at this stage also a bit different. Whereas simulations appear to have three maximum points, experiments only show one (maybe two small ones). This could be attributed to the number of measurement points making it imperceptible. Or it could be the fact that the mixing from jet streams have developed to a level making the wake more uniform. It would seem logical to get one peak for each rotor in width but at this stage, the wake has perhaps regenerated already to a point where the centre of the wake is more uniform. This makes sense when looking at the centreline in Figure 4-3 (a), where MR7 already has regained a lot by 2D. It is also worth mentioning that computational simulations do not always perceive all physical phenomena correctly. Moving on to 4D there is once again little that separates the two. The simulation has regained around 5% landing at 40% total, whereas the experiment regained 20% ending up at 50%. There is a significant turning point between them once they reach 7D. At this point, the experiment has surpassed the simulation, with a deficit of only 25% compared to 30%. Even so, they both end up equal at 10D and 20%. There are no current turbulence intensity plots from Bastankhah et al. regarding MR7. Turbulence is therefore not compared.

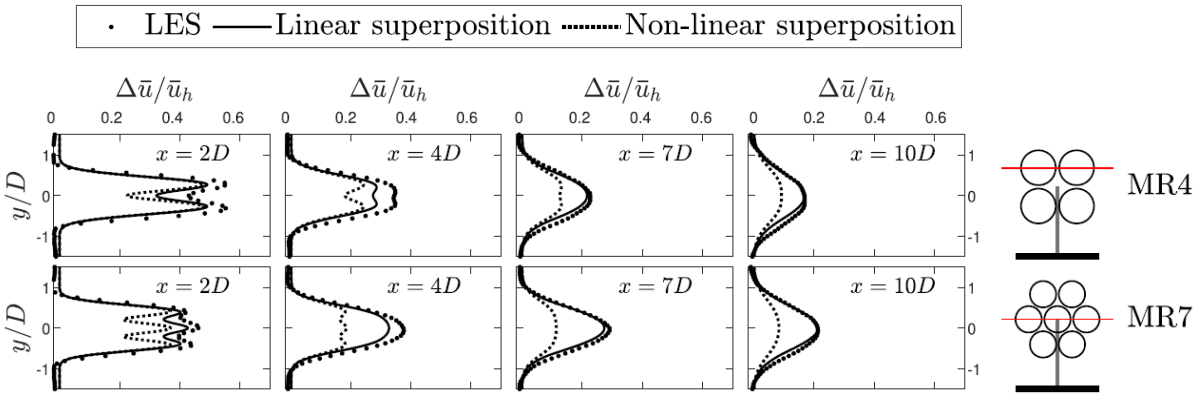

Figure 5-3: MR7 wake simulation from Bastankhah et al. (2019) showing offset measurement from MR4 (top) and centre measure MR7 (bottom).

The velocity deficit profiles from LES and experimental results, mostly have similar shapes at the different downstream distances. In the near wake region at 2D, LES has lower velocity deficits compared to the experimental results. This is also a fact for 4D downstream, but the

change is slightly evened out at this distance, especially for the MR7 and single-rotor setup. In the far wake at 7D and 10D, the differences are rather minimal. For the turbulence intensity, both shape and value were almost equal for the single-rotor in the near wake. The differences appear when comparing the MR4. Notably, the turbulence seems to be recovering at an earlier stage in the simulations. When reviewing the experimental results, it may appear to be little that separates MR4 and MR7 regarding velocity deficit and in the simulation, it can also seem negative to increase the number of rotors. However, it has to be kept in mind that MR4 is measured at the centre where free stream flow is let through and is therefore likely to have artificially low velocity deficit levels. Wake measurements from MR4 can as a result be more reasonable to conduct at both OC and TC. A short centreline was in our study done for the OC in Figure 4-7 to show that there are noticeable differences, especially in the near wake. But a more thorough wake simulation was performed by Bastankhah et al. Their results presented at the top in Figure 5-3, demonstrate that when measuring in OC the velocity deficit is larger than for MR7 in the near wake. It is therefore reasonable to believe that an increase in rotor number does decrease the velocity deficit, but it is difficult to conclude with the limited data.

There are several possible reasons for the variations in the results. The simulations are done with other presuppositions like incoming turbulence intensity and disc rotation that could lead to differences for the wake recovery, especially in the near wake. When having turbulence and shear in the inlet and freestream flow, the wake could be fuelled by turbulence both at the start and along the sides further downstream. And thereby not getting the same major shear gradients in the vicinity of free stream flow. This is probably also the reason why turbulence reduction is slower and more constant in the simulations. It is therefore reasonable to believe that the major differences in velocity deficit are at least partly because of the turbulence settings. This does make sense according to the findings of Bastankhah et al. [10], where transition length is a function of spacing and inlet turbulence. By increasing the incoming turbulence, the transition length was found to be reduced. Therefore, since our experiment is performed with zero turbulence in contrast to the simulations 6.7%, deficits are more significant at the start whereas recovery gradients are higher. Although seeing that the far wake is rather similar for all test subjects, it could imply that factors like incoming turbulence intensity have less influence on wake recovery at longer downstream distances. Also, the tip vortices from rotation have dissolved and decayed in the transition region and therefore contributing to less mixing in the far wake region. It is in addition worth mentioning that the turbulence intensity is only based on standard deviation in x direction, unlike turbulent kinetic energy which uses both x, y, and z direction. This could be important and affect the results in the near wake, where it is yet to be isotropic. Considering how different the turbulence plots are for single-rotor and MR4 it would be interesting to also compare MR7, but data is not available for the time being. Another possible contributor to dissimilarities is the use of different types of actuator discs. The solidity, thrust, and radial thrust force distribution from the discs control the flow. A lower solidity or thrust coefficient would therefore lead to higher flow and lower velocity deficits. In our experimental setup, the discs were measured to have a thrust coefficient of approximately 0.87 [12], whereas Bastankhah et al. simulated discs with 0.8 ± 0.02. The difference is not necessarily that substantial, but still enough to possibly provide noticeably different results. A simulation is also fully dependent on the chosen parameters, where a lot of assumptions are

made. Changing just a fraction of the parameters could alter the results completely. The structure of the multi-rotor turbines from the experiment could to some extent impinge the results. Given that the joints occupy space behind the rotor, and the staffs block the flow. Nevertheless, the flow in the disc centre is only marginal, and realistically a full-scale rotor hub would fill this same void. If anything, it only makes it more genuine, although it differs from the simulation.

5.2 Effect of rotor spacing

In our experiment, MR7 was measured with different inter-rotor spacings. Both wake and centrelines were recorded with a spacing of 0.0D, 0.1D, and 0.4D. Similar simulations were also done for Bastankhah et al. with MR4 instead. Only the difference is that 0.4D spacing was substituted with 0.25D and no wake simulations were recorded, only centrelines. It is important to note that these centrelines are averaged over the rotors and not just a turbine centre recording like in the experiment. The results can therefore not be directly compared but give insight into noticeable trends. Our findings showed that increasing the spacing has a major impact on the velocity deficit. In Figure 4-4 (a) the difference between 0.0D and 0.4D spacing is almost 40% at a downstream distance of 2D. Although this deficit gap minimizes further downstream, rotor spacing does likely affect the near wake velocity deficit positively. The work from Bastankhah et al. supports this statement, as they reached the same conclusion based on the simulation results given in Figure 5-4.

> *"The LES results of MR turbine wakes for different values of rotor spacing showed that wakes of MR turbines with larger rotor spacing are characterized by lower values of velocity deficit. This was explained by the fact that the increase in rotor spacing postpones the wake transition to a single wake."*

One difference in their results is the downstream distance at which velocity deficit contrast are the highest. In the experimental data in Figure 4-5 curves started separating at a distance of 1D and merged at 4D, while the highest measured difference is located around 2D. In contrast, for the simulation results, separation happened at the same point but did not completely merge before 12D. It also had its most substantial dissimilarity located at 3D. It is hard to locate any exact reasons why our data and the simulations do not portrait the same result, based only on a centreline with other conditions. Nevertheless, the important part is the trend at which they are showing. Where both studies find a decrease in velocity deficit, with increased spacing.

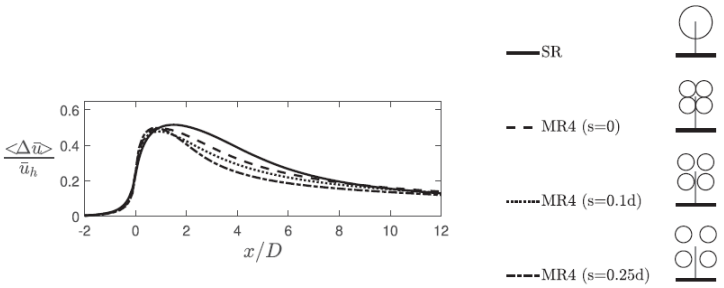

FIG. 12. Variation of the normalized velocity deficit, averaged over the rotors, $\langle \Delta \tilde{u} \rangle / \tilde{u}_h$ with the streamwise distance for the SR turbine as well as the MR turbines with different values of rotor spacing.

Figure 5-4: MR4 centreline simulation from Bastankhah et al. (2019) showing different inter-rotor spacings.

5.3 Vestas MR4 and a wind farm comparison

Field measurements and numerical simulations are performed by vdLaan et al. [7] on the wake of the Vestas MR4 turbine. The horizontal and vertical spacing between rotors is at 0.064D and 0.043D. Figure 5-5 shows wake measurement and simulation results of the Vestas MR4 turbine at a downstream distance of 1D. Windscanner measurements are illustrated by the black curve, whereas the rest are different types of simulations. Field measurements deviate slightly from simulations, especially in the near wake region. The wake velocity deficit from simulations is almost 10% at the centre of the turbine and 30% on the sides. Meanwhile, the windscanner measures 30% in the centre and 40% on the sides. From centreline measurements in Figure 4-3 (a) there is measured a velocity deficit of approximately 15%, but there is no wake profile measured at this downstream distance making it hard to compare. vdLaan et al. [7] point out that one reason for the difference between simulations and windscanner measurements is the fact that the incoming windspeed used in simulations is measured at a location approximately 200m away from the turbine. The difference in velocity deficit between our results and windscanner measures, could be due to the smaller spacing between the Vestas rotors. This probably causes the velocity deficit to be higher for the windscanner measurements compared to our results. Note that this is only a comparison with the centreline measurements and does not represent the entire wake.

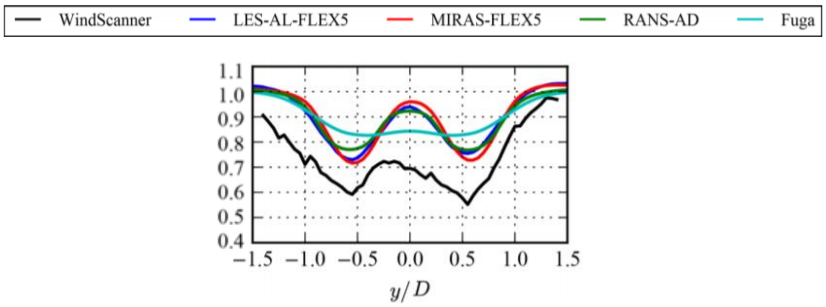

Figure 5-5: Wake profiles at 1D adapted from vdLaan et al. (2019) showing normalised velocity deficit.

Figure 5-6 shows wake measurement and simulation results of the Vestas MR4 turbine at a downstream distance of 2.75D and 6D. At a downstream distance of 2.75D the maximum velocity deficit is at 30% for windscanner measurements, while our results show approximately 70% at a downstream distance of 2D and 50% at 4D in Figure 4-1 (a). Compared with centreline measurements in Figure 4-3 (a) there is a velocity deficit of 55% at 2.75D downstream. Many elements could contribute to these differences. Seeing that the windscanner measurements are performed on an onshore wind turbine, incoming turbulence is most likely one of the main factors. With no incoming turbulence in our experiment, shear gradients are probably higher causing our MR4 to have a greater and more distinct maximum velocity deficit. Further back at 6D downstream there is no windscanner data but results from different types of simulation average around 17% for the velocity deficit. Compared against the experimental results peaking at 30% for a downstream distance of 7D. Both our results and results from vdLaan et al. [7] show lower velocity deficits for the Multi-rotor compared to the single-rotor.

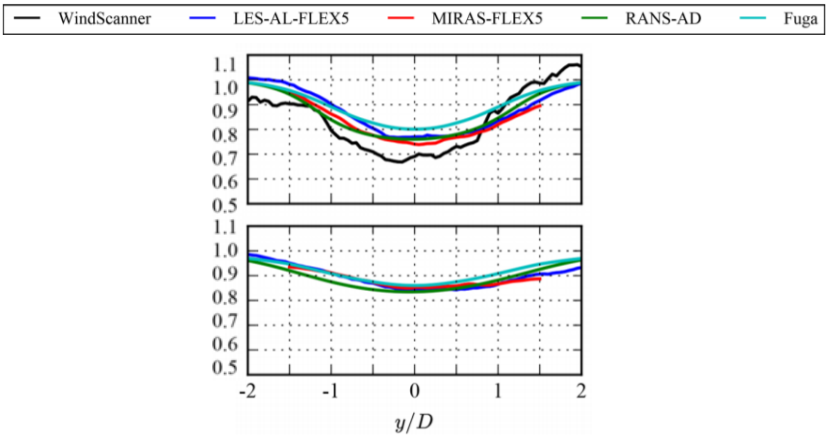

Figure 5-6: Wake profiles at 2.75D and 6D adapted from vdLaan et al. (2019) showing normalised velocity deficit.

vdLaan et al. [8] have also performed RANS simulation of a 4x4 MR4 wind farm compared against a single-rotor wind farm of equivalent size. Their simulations are performed using non-rotating actuator discs with a spacing of 0.05D. The different test scenarios include downstream spacing between each turbine row of 3D, 4D and 5D. Simulation and experimental results both show faster wake recovery for the multi-rotor turbine, which could lead to closer spacing of wind farms. In this case, it is also worth mentioning that simulations are performed with incoming turbulence, which is realistic in a wind farm. If this were included in the experiment it would probably have led to faster wake recovery. Simulations show that the largest difference in inflow speed due to wake effects is experienced by the second row of turbines. For the turbine rows further downstream the velocity deficit is measured to be similar for the rows of single-rotor and multi-rotor turbines.

6 Conclusion

Experimental wake measurements have been performed at HVL's Marine lab, where different multi-rotor setups have been tested to analyse the wake characteristics. Simplified actuator disc models were used to generate satisfying baseline results for further experimenting and comparison with computational simulations. Previous work on a single-rotor wake allowed for comparisons to study the effect of rotor number and spacing. Where the main objective of this study was to find if multi-rotor systems could be advantageous concerning faster recovery and lower velocity deficit in the wake. Our results show that an increase in rotor number can have a significant effect, especially on the near wake. The presence of additional jet streams in between the rotors of a multi-rotor makes the wake regenerate faster. This contributes to lower deficits than for the single-rotor. However, the far wake is rather similar for all test cases but is slightly in favour of the single-rotor. Due to higher mixing in the near wake, multi-rotors recovers quickly to a uniform wake. A side effect is that the development of turbulence along the centrelines behind the multi-rotor setups initially shows stronger gradients, which then flattens out with increasing downstream distance. The single-rotor will as a result regain larger quantities for each step until it surpasses the multi-rotors. Further testing with other multi-rotor setups needs to be performed, to find if there is a direct link between increasing rotor number and reduced deficits.

The impact of inter-rotor spacing is in this study found to have a profound effect on wakes. By increasing the distance between each rotor, mixing is greatly increased. Meaning the wakes are uniform at an earlier distance. This correlates to lower velocity deficits and rapidly decreasing turbulence in the vicinity of the turbine. While this is an important feature in the near wake, it is at the expense of the far wake where deficits are presumably higher. Our results also found that with no spacing, the multi-rotor is almost identical to the single-rotor. Spacing and downstream distance is therefore key to fully take advantage of the multi-rotors.

Depending on the downstream spacing of wind turbines, multi-rotors could indeed be a positive contribution to wind farms. Considering area efficiency is important to maximise the power output and economic profit, multi-rotors may reduce the needed spacing. By taking into account that a turbine is usually installed at a distance of 5-8D, some extreme cases have the potential to shorten the spacing by as much as half the distance between the first two rows of turbines. At the same time, this would yield lower fatigue loads due to turbulence. Although, our lab-scale results are recorded under ideal conditions and thus not directly comparable to full-scale wind turbines with atmospheric boundary layers. For future work, it will be reasonable to include grids in the tank to find the effect of inlet turbulence. As we suspect the advantages of multi-rotors to reduce when increasing the turbulence. It is also interesting to conduct experiments on axial forcing on multi-rotors in a wind farm arrangement, where multi-rotors are placed behind each other. This would be a logical next step in building up a more realistic scenario.

References

[1] European comission, 'Boosting Offshore Renewable Energy', *European Commission*, Nov. 19, 2020. https://ec.europa.eu/commission/presscorner/detail/en/ip_20_2096 (accessed Feb. 01, 2021).

[2] European comission, 'Onshore and offshore wind', *European Commission*, Apr. 21, 2020. https://ec.europa.eu/energy/topics/renewable-energy/onshore-and-offshore-wind_en (accessed Feb. 01, 2021).

[3] P. Jamieson and M. Branney, 'Multi-Rotors; A Solution to 20 MW and Beyond?', *Energy Procedia*, vol. 24, pp. 52–59, 2012, doi: 10.1016/j.egypro.2012.06.086.

[4] P. Jamieson and M. Branney, 'Structural Considerations of a 20MW Multi-Rotor Wind Energy System', *J. Phys. Conf. Ser.*, vol. 555, Dec. 2014, doi: 10.1088/1742-6596/555/1/012013.

[5] S. Störtenbecker, P. Dalhoff, M. Tamang, and R. Anselm, 'Simplified support structure design for multi-rotor wind turbine systems', *Wind Energy Sci.*, vol. 5, no. 3, pp. 1121–1128, Aug. 2020, doi: https://doi.org/10.5194/wes-5-1121-2020.

[6] C. H. Linde, '4-Rotor Concept Turbine', *DTU Wind Energy*. https://www.vindenergi.dtu.dk/english/research/research-facilities/konceptmoellen (accessed Feb. 08, 2021).

[7] M. P. van der Laan *et al.*, 'Power curve and wake analyses of the Vestas multi-rotor demonstrator', *Wind Energy Sci.*, vol. 4, no. 2, pp. 251–271, May 2019, doi: 10.5194/wes-4-251-2019.

[8] M. P. van der Laan and M. Abkar, 'Improved energy production of multi-rotor wind farms', *J. Phys. Conf. Ser.*, vol. 1256, Jul. 2019, doi: 10.1088/1742-6596/1256/1/012011.

[9] N. S. Ghaisas, A. S. Ghate, and S. K. Lele, 'Large-eddy simulation study of multi-rotor wind turbines', *J. Phys. Conf. Ser.*, vol. 1037, Jun. 2018, doi: 10.1088/1742-6596/1037/7/072021.

[10] M. Bastankhah and M. Abkar, 'Multirotor wind turbine wakes', *Phys. Fluids*, vol. 31, no. 8, Aug. 2019, doi: 10.1063/1.5097285.

[11] S. de J. Helvig, M. K. Vinnes, A. Segalini, N. A. Worth, and R. J. Hearst, 'A comparison of lab-scale free rotating wind turbines and actuator disks', *J. Wind Eng. Ind. Aerodyn.*, vol. 209, Feb. 2021, doi: https://doi.org/10.1016/j.jweia.2020.104485.

[12] M. Hansen, C. Leikvoll, and M. Vikse, 'Multirotor wind turbine-drag', Høgskulen på Vestlandet, Bergen, Bachelor oppgave, May 2021.

[13] P. Brøndsted and R. P. L. Nijssen, '3.2.1 One-Dimensional Momentum Theory', in *Advances in Wind Turbine Blade Design and Materials*, Woodhead Publishing, 2013, pp. 63–67.

[14] S. P. Neill and M. R. Hashemi, 'Tidal Energy', in *Fundamentals of Ocean Renewable Energy - Generating Electricity from the Sea*, Elsevier, 2018, pp. 47–81.

[15] T. Nishino and R. H. J. Willden, 'The efficiency of an array of tidal turbines partially blocking a wide channel', *J. Fluid Mech.*, vol. 708, pp. 596–606, 2012, doi: 10.1017/jfm.2012.349.

[16] S. McTavish, D. Feszty, and F. Nitzsche, ‘A study of the performance benefits of closely-spaced lateral wind farm configurations’, *Renew. Energy*, vol. 59, pp. 128–135, Nov. 2013, doi: 10.1016/j.renene.2013.03.032.

[17] A. R. Meyer Forsting, N. Troldborg, and M. Gaunaa, ‘The flow upstream of a row of aligned wind turbine rotors and its effect on power production’, *Wind Energy*, vol. 20, no. 1, pp. 63–77, 2017, doi: https://doi.org/10.1002/we.1991.

[18] D. Coiro and T. Sant, ‘The future of offshore wind turbine technology’, in *Renewable Energy from the Oceans - From Wave, Tidal and Gradient Systems to Offshore Wind and Solar*, Institution of Engineering and Technology, 2019, pp. 230–232.

[19] P. Chasapogiannis, J. M. Prospathopoulos, S. G. Voutsinas, and T. K. Chaviaropoulos, ‘Analysis of the aerodynamic performance of the multi-rotor concept’, *J. Phys. Conf. Ser.*, vol. 524, Jun. 2014, doi: 10.1088/1742-6596/524/1/012084.

[20] B. Sørensen, ‘Individual renewable energy sources’, in *Renewable Energy - Physics, Engineering, Environmental Impacts, Economics and Planning (5th Edition)*, 5th ed., Elsevier, 2018, pp. 219–343.

[21] ‘Turbulence intensity’. https://www.cfd-online.com/Wiki/Turbulence_intensity (accessed May 12, 2021).

[22] M. Ge, D. Tian, and Y. Deng, ‘Reynolds Number Effect on the Optimization of a Wind Turbine Blade for Maximum Aerodynamic Efficiency’, *J. Energy Eng.*, vol. 142, no. 1, Mar. 2016, doi: 10.1061/(ASCE)EY.1943-7897.0000254.

[23] ‘Vectrino — Nortek International’. http://195.62.126.26/en/products/velocimeters/vectrino (accessed Feb. 22, 2021).

[24] J. R. Bjørnsen, ‘Blockage and wake effects for multiple actuator discs with lab-scale measurements’, Universitetet i Bergen, Bergen, May 2021.

List of figures